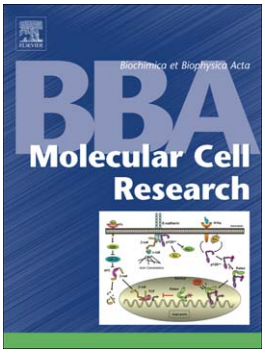

Zonula occludens-2 regulates Rho proteins activity and the development of epithelial cytoarchitecture and barrier function

Arturo Raya-Sandino, Alejandro Castillo-Kauil, Alaide Domínguez-Calderón, Lourdes Alarcón, David Flores-Benitez, Francisco Cuellar-Perez, Bruno López-Bayghen, Bibiana Chávez-Munguía, José Vázquez-Prado, Lorenza González-Mariscal

PII: S0167-4889(17)30141-6
DOI: doi:10.1016/j.bbamcr.2017.05.016
Reference: BBAMCR 18102

To appear in: *BBA - Molecular Cell Research*

Received date: 18 August 2016
Revised date: 18 May 2017
Accepted date: 24 May 2017

Please cite this article as: Arturo Raya-Sandino, Alejandro Castillo-Kauil, Alaide Domínguez-Calderón, Lourdes Alarcón, David Flores-Benitez, Francisco Cuellar-Perez, Bruno López-Bayghen, Bibiana Chávez-Munguía, José Vázquez-Prado, Lorenza González-Mariscal, Zonula occludens-2 regulates Rho proteins activity and the development of epithelial cytoarchitecture and barrier function, *BBA - Molecular Cell Research* (2017), doi:10.1016/j.bbamcr.2017.05.016

Zonula occludens-2 regulates Rho proteins activity and the development of epithelial cytoarchitecture and barrier function

Arturo Raya-Sandino[1], Alejandro Castillo-Kauil[6], Alaide Domínguez-Calderón[1], Lourdes Alarcón[1], David Flores-Benitez[3], Francisco Cuellar-Perez[1], Bruno López-Bayghen[4], Bibiana Chávez-Munguía[4], José Vázquez-Prado[2] and Lorenza González-Mariscal[1]

[1]Department of Physiology, Biophysics and Neuroscience, Center for Research and Advanced Studies (Cinvestav), México D.F., 07360, México.
[2]Department of Pharmacology, Center for Research and Advanced Studies (Cinvestav), México D.F., 07360, México.
[3]Max-Planck-Institute of Molecular Cell Biology and Genetics, 01307-Dresden, Germany
[4]Department of Toxicology, Center for Research and Advanced Studies (Cinvestav), México D.F., 07360, México.
[5]Department of Infectomics and Molecular Pathogenesis, Center for Research and Advanced Studies (Cinvestav), México D.F., 07360, México.
[6]Department of Cell Biology, Center for Research and Advanced Studies (Cinvestav), México D.F., 07360, México.

Corresponding Author
Lorenza González-Mariscal PhD
Department of Physiology, Biophysics and Neuroscience,
Center for Research and Advanced Studies (Cinvestav),
Ave IPN 2508,
México D.F., 07360,
México.
lorenza.goma@gmail.com
Fax:5255-5747-3996
Tel:5255-5747-3966

Abstract
Silencing Zonula occludens 2 (ZO-2), a tight junctions (TJ) scaffold protein, in epithelial cells (MDCK ZO-2 KD) triggers: 1) Decreased cell to substratum attachment, accompanied by reduced expression of claudin-7 and integrin β1, and increased vinculin recruitment to focal adhesions and stress fibers formation; 2) Lowered cell-cell aggregation and appearance of wider intercellular spaces; 3) Increased RhoA/ROCK activity, mediated by GEF-HI recruitment to cell borders by cingulin; 4) Increased Cdc42 activity, mitotic spindle disorientation and the appearance of cysts with multiple lumens; 5) Increased Rac and cofilin activity, multiple lamellipodia formation and random cell migration but increased wound closure; 6) Diminished cingulin phosphorylation and disappearance of planar network of microtubules at the TJ region; and 7) Increased transepithelial electrical resistance at steady state, coupled to an increased expression of ZO-1 and claudin-4 and a decreased expression of claudin-2 and paracingulin. Hence, ZO-2 is a crucial regulator of Rho proteins activity and the development of epithelial cytoarchitecture and barrier function.

Key words: Tight junction, ZO-2, Rho GTPases, cofilin, cingulin, GEF-H1

Introduction

In multicellular organisms, epithelia constitute the frontier between the *interior milieu* and the environment. Epithelial cells display as a distinguishing feature, at the uppermost portion of their lateral membranes, a structure called tight junction (TJ) that regulates the passage of ions and molecules through the paracellular pathway. TJs are formed by various integral proteins like occludin, tricellulin and JAMs that establish cell-cell contact at the intercellular space, and by claudins that form the paracellular pores or barriers responsible for ionic selectivity in each tissue (for review see [1].

These transmembrane proteins are associated at the cytoplasmic face with a complex array of proteins, including cingulin, paracingulin and several members of the family of membrane-associated guanylate kinase homologs (MAGUK) [for review see [2, 3]]. This family includes the Zonula occludens (ZO) proteins ZO-1, -2 and -3, which contain PDZ, SH3 and GUK domains that allow them to bind to a wide variety of proteins, including the integral proteins of the TJ [4-8], connexins of gap junctions [9-12], α-catenin of adherens junctions [13], and signaling molecules like kinases [14]. In addition, these proteins contain actin-binding regions that associate to actin [15, 16] and to actin binding proteins like 4.1 [17] and cortactin [18]. This configuration thus allows ZO proteins to act as bridges that physically link transmembrane TJ proteins to the apical cytoskeleton of F-actin and myosin II (actomyosin).

The movement of ions and molecules through the TJ depends on both the charge and size of the solute. Those smaller than 4 A^{o} in radius, pass through claudin based pores [19, 20], whereas larger solutes move as the contractile tone of the apical cytoskeleton increases and expands the intercellular space (for review see [21]). The contractility of the actomyosin apical ring is regulated by protein RhoA [22] that activates Rho kinase (ROCK), which phosphorylates the myosin II regulatory light chain (MLC2) [23]. In addition, MLC2 is phosphorylated by the MLC kinase (MLCK) [24], and ROCK can increase MLC2 phosphorylation through an indirect way, by the phosphorylation and consequent inactivation of MLC phosphatase [25].

Rho proteins, RhoA, Cdc42 and Rac, are small guanosine triphosphate (GTP)-binding molecules that switch between a GDP-bound or inactive state and a GTP-bound or active conformation. Switching between these two conditions is regulated by guanine nucleotide exchange factors (GEF) and GTPase activating proteins (GAPs). RhoA regulates both the contractility of the actomyosin apical ring [22] and TJ assembly [26]. RhoA inhibition either has no effect on TJ morphology and TJ protein distribution [27], or triggers a decreased localization of junctional components at the membrane [26]. In correspondence, a constitutive Rho signaling favors the accumulation of TJ proteins at cell junctions and protects TJ during ATP depletion [26], or can also induce a dramatic disorganization of TJ strands and protein distribution [27]. Therefore, a balance between the amount of active and quiescent RhoA appears to be crucial for the formation and stability of TJ.

ZO-2 is a 160 kD MAGUK protein with a dual localization. Thus in quiescent epithelial cells ZO-2 is present at the TJ, whereas in proliferating cells it localizes both at the TJ and the nucleus [28]. At the nucleus, ZO-2 accumulates in speckles, co-localizes with the essential splicing factor SC-35, and inhibits gene transcription by

association to molecular complexes formed by transcription factors and histone deacetylases [29, 30]. The movement of ZO-2 between the nucleus and the TJ is controlled by several nuclear localization and exportation signals [31] that are regulated by posttranslational modifications including phosphorylation [32] and O-N-acetyl glycosylation [33].

The presence of ZO-2 at both the nuclei and the cytoplasmic face of the plasma membrane, together with the vast amount of proteins that associate to ZO-2 (for review see [3], have driven the interest to silence ZO-2 in order to detect processes where the expression of this protein is essential. In this respect, previously it had been found that silencing of both ZO-1 and ZO-2 impairs the polymerization of claudins into TJ strands [34], revealing a redundant and fundamental role of these MAGUK proteins in TJ strand formation. In humans, the mutations in ZO-2 gene (*TJP2*) have been associated to familial hypercholanemia, a disease characterized by leakage of bile into serum [35], and in chimeric mice, the lack of ZO-2 severely affects male fertility, as the blood-testis barrier is breached despite the correct expression of other TJ proteins [36]. These results thus revealed the seminal role of ZO-2 in sealing the TJs of the biliary ducts and testis.

Here we have employed a stable ZO-2 knock down (KD) MDCK cell line, to identify phenotypic changes that could pinpoint processes in which the participation of ZO-2 is crucial. We found that the lack of ZO-2 triggers: 1) A decrease in cell to substratum attachment accompanied by a diminished expression of claudin-7 and integrin $\beta 1$, and reinforcement of adhesion sites by vinculin recruitment and profusion of stress fibers; 2) Lowered cell-cell aggregation coupled to the appearance of wider intercellular spaces; 3) Increased activity of RhoA/ROCK and actin-myosin contractility, mediated by cingulin recruitment to the cell borders of GEF-H1; 4) Increased activity of Cdc42 accompanied by mitotic spindle disorientation and the appearance of cells growing on top of each other in 2 dimension (D) cultures and of multiple lumens per cyst in 3D cultures; 5) Increased Rac and cofilin activity that correlates with the formation of multiple lamellipodia that induce random cell migration, instead of directional migration, but increase the velocity of wound closure; 6) A decrease in cingulin phosphorylation followed by the disappearance of the planar network of microtubules at the TJ region; and 7) Increased transepithelial electrical resistance (TER) and lowered paracellular permeability, coupled to an increased expression of ZO-1 and claudin-4 and a decreased expression of claudin-2 and paracingulin. Altogether, our results indicate that ZO-2 is important to regulate the activity of Rho proteins, for proper cell architecture to develop and for TJ formation and sealing.

Materials and Methods

Cell culture and Ca-switch assay

Parental (control) and ZO-2 KD MDCK II cells were kindly provided by Alan Fanning (University of North Carolina, Chapel Hill, NC) and cultured as previously described [37]. Three clones of ZO-2 KD cells were used in this study: IC5, IC6 and 2D1. All of

them stably expressed a mixture of three different shRNAs against ZO-2 in the pSuper vector. Parental cells instead, only expressed the empty vector. Stable clonal MDCK cell lines were isolated on the basis of zeocin resistance. The phenotype was rescued upon transfection of ZO-2 KD cells with a human full length ZO-2 construct with altered shRNA binding sites (pTRE-hZO-2; generously provided by Dr. Alan Fanning of the University of North Carolina). Sparse and confluent cultures were respectively plated at a density of 1.5 x 10^5 cells/cm^2 and 5 x 10^5 cells/cm^2.

For the Ca-switch assay, parental and ZO-2 KD cells were plated at sparse density (1.5 x 10^5 cells/cm^2) on Transwell filters or glass coverslips according to the experimental needs. When the monolayers had acquired confluence 48 h later, the cultures were gently washed 5 times with PBS without Ca^{2+} and incubated in low Ca^{2+} (LC) medium (1-5 μM Ca^{2+}). After 20 h in LC medium, the monolayers were switched to normal calcium medium (1.8 mM Ca^{2+}) for different periods of time.

Cell transfections

ZO-2 KD cells were plated in 24-well plates at a density of 5x10^4 cells/well. One day later they were transfected with Lipofectamine™ 2000 (Life Technologies, Cat. 11668-019, Carlsbad, CA) with the following constructs: 0.4 μg of pTRE-hZO-2 resistant to the anti ZO-2 shRNAs employed (generously provided by Dr. Alan Fanning, University of North Carolina, Chapel Hill, USA); or 0.5 μg of p-EGFP (Clontech, Cat. 6085-1, Palo Alto, CA) and 0.4 μg of pCDNA-EGFP-GEF-H1 Y393A (generously provided by Dr. Celine DerMardirossian, from the Department of Immunology and Microbial Science, and the Department of Cell and Molecular Biology of the Scripps Research Institute, CA, USA). ZO-2 parental cells plated at sparse density were transfected with Lipofectamine™ 2000 with 0.5 μg of p-EGFP (Clontech, Cat. 6085-1, Palo Alto, CA) and 0.4 μg of construct pCDNA-EGFP-GEF-H1 C53R (generously provided by Dr. Celine DerMardirossian).

Immunofluorescence

Immunofluorescence was done following standard procedures as described previously [38] using the following primary antibodies: rabbit polyclonals against ZO-2 (Invitrogen, Cat. 711400, dilution 1:100, Carlsbad, CA), myosin IIa (Covance, Cat. PRB-445P; dilution 1:100, Berkeley, CA), phospho myosin light chain kinase 2 (p-MLC2 Ser 20) (Abcam, Cat. Ab2480, dilution 1:100, Cambridge, MA), β-tubulin coupled to FITC (Sigma Aldrich, Cat. F2043, dilution 1:50, St. Louis, MO), claudin-1 (Invitrogen, Cat. 51-9000, dilution 1:50, Camarillo, CA) and claudin-7 (Invitrogen, Cat. 34-9100¸dilution 1:50, Camarillo, CA); and mouse monoclonals against gp135/podocalyxin (Invitrogen, Cat. 39-3800, dilution 1:100, Camarillo, CA), GEF-H1 (Abcam, Cat. Ab90783, dilution 1:5, Cambridge, MA), and β-tubulin (Sigma Aldrich, Cat. T7816; dilution 1:5000, St Louis, MO), as well as a rat monoclonal against E-cadherin (Sigma-Aldrich, Cat U3254; dilution 1:100, St Louis, MO), a rabbit monoclonal against p-cofilin (Ser3) (Cell Signaling Technology, Cat. 3313; dilution 1:1000; Danvers, MA) and a mouse monoclonal against β-tubulin (sigma-Aldrich, Cat T7816; dilution 1:500, St Louis, MO). As secondary antibodies we employed donkey

antibodies against rabbit IgG coupled to Alexa Fluor 594 (Invitrogen, Cat A21207, dilution 1:100, Carlsbad, CA) and against mouse IgG coupled to Alexa Fluor 594 (Invitrogen, Cat A21203, dilution 1:100, Carlsbad, CA) or to Alexa Fluor 488 (Life Technologies, Cat A11001, dilution 1:100, Eugene, OR), as well as a rabbit antibody against rat IgG coupled to FITC (Sigma-Aldrich, Cat. F1763, St. Louis MO). Rhodaminated phalloidin (Invitrogen, Cat R415, 1:50, Eugene, OR) was employed for the detection of F-actin.

In the experiment with inhibitors ML-7 and Y27632, these drugs were added to confluent monolayers and after 30 min, the monolayers were washed thrice with PBS, fixed and processed for immunofluorescence. The C3 inhibitor was added for 2 h to confluent monolayers cultured in serum free media, the monolayers were washed thrice with PBS, fixed and processed for immunofluorescence.

MDCK ZO-2 KD cells have a bigger size than parental cells, since the lack of ZO-2 induces hypertrophy [39]. Therefore although the former cells might look bigger in the immunofluorescence images of this work, they were taken at the same magnification as parental cells, as indicated in each figure.

Western blot

Western blots were done following standard procedures [33] and employing the following mouse monoclonal antibodies against ROCK II (BD Biosciences, Cat. 610623, dilution 1:2000, San Jose, CA), GEF-H1 (Abcam, Cat. Ab90783, dilution 1:50, Cambridge, MA); integrin β4 (BD Biosciences, Cat. 611233, dilution 1:500, Franklin Lakes, NJ) β-tubulin (Sigma Aldrich, Cat. T7816, dilution 1:20,000, Saint Louis, MO) and actin (generated and generously provided by Dr Manuel Hernández, Cinvestav, Department of Cell Biology); and the following rabbit polyclonals against ZO-2 (Invitrogen, Cat. 711400, dilution 1:1000, Carlsbad, CA), phospho myosin light chain kinase 2 (p-MLC2 Ser 20) (Abcam, Cat. Ab2480, dilution 1:5000, Cambridge, MA), myosin IXb (Sigma Aldrich, Cat. M5566, dilution 1:2000, St. Louis, MO); claudin-7 (Invitrogen, Cat. 34-9100, dilution 1:250, Camarillo, CA), integrin β1 (Millipore, Cat. AB1952, dilution 1:1000, Billerica, MA) and ROCK I (Chemicon International, Cat. AB3885, dilution 1:3000, Warford, United Kingdom). As secondary antibodies we employed a goat anti rabbit IgG coupled to peroxidase (Sigma Aldrich, Cat A9169, dilution 1:10,000, San Louis, MO)., followed by a chemiluminescence detection system (Immobilon™ Western, Millipore Corporation, Cat. WBKLS 0500, Billerica, MA).

For the mobility shift detection assay of phosphorylated proteins, a phosphate affinity SDS-PAGE was done with acrylamide-pendant Phos-tag ligand (Waco Pure Chemical Industries, Cat. AAL-107, Richmond, VA).

Semithin sections

Samples were fixed with 2.5% glutaraldehyde in 0.1 M sodium cacodylate buffer pH 7.2 for 60 min and postfixed with 1% osmium tetroxide in the same buffer for 60 min. Samples were dehydrated with increasing concentrations of ethanol and propylene oxide. Afterwards, they were embedded in Polybed epoxy resins and polymerized at 60°C for 24 h. Semithin sections (500 nm thick) were obtained and stained with

toluidin blau (Sigma) and observed in an Axiophot photo-microscope (Carl Zeiss, Germany) equipped with a Zeiss AxioCam MRc digital camera (Carl Zeiss Vision GmbH, Germany).

Rho proteins activation assays

RhoA activity was measured by G-LISA™ assay (Cytoskeleton, Cat BK124, Denver, CO) done on cell extracts derived from control and ZO-2 KD MDCK cells. Absorbance was read at 490 nm.

Activation of Cdc42 and Rac1 in parental and ZO-2 KD cells and of RhoA in ZO-2 KD cells transfected with a hZO-2 construct, non-sensitive to the shRNA against ZO-2, was assessed by detecting in a pulldown assay, as previously described [40], the interaction of the Rho proteins with GST fusion proteins that contain their effector protein domains: CRIB domain of PAK for Cdc42 and Rac1, and RBD domain of Rhotekin for RhoA. MDCK cells were washed with PBS containing 10 mM $MgCl_2$ and lysed with 1 ml of ice-cold lysis buffer (50 mM Tris, 150 mM NaCl, pH 7.5, containing 1% Triton X-100, 5 mM EDTA), protease inhibitors (1 mM phenylmethylsulfonyl fluoride, 10 μg/ml leupeptin, and 10 μg/ml aprotinin), and phosphatase inhibitors (1 mM NaF, 1 mM sodium orthovanadate, and 1 mM glycerolphosphate), containing 10 mM $MgCl_2$. Cell lysates were incubated with 40 μl of GST-PAK CRIB or GST-Rhotekin RBD beads on ice for 45 min on a shaker. Beads were then centrifuged at 5,000 rpm for 2 min and washed with lysis buffer. Beads were then resuspended in 35 μl of 1X Laemmli buffer, boiled for 5 min, centrifuged at 13,000 rpm for 5 min. Beads were then resolved in 12% acrylamide, transferred to PVDF membranes, and immunoblotted using anti-Cdc42 (Santa Cruz Biotechnology Inc. Cat. sc-87, dilution 1:5,000), anti-Rac1 (Santa Cruz Biotechnology Inc. Cat. sc-217, dilution 1:40000) or anti-RhoA (Santa Cruz Biotechnology Inc. Cat. sc-418, dilution 1:5000) monoclonal antibodies. As controls, total cell lysates were analyzed in parallel.

Spatiotemporal dynamics of RhoA activation

For this purpose we employed a single-chain biosensor previously described [41] that responds to RhoA activation (Addgene, plasmid 12150, Cambridge, MA) and consists of a Rho-binding domain of the effector rhotekin (RBD) which specifically binds to GTP-RhoA, followed by cyan fluorescent protein (CFP), a linker of optimized length, a pH-insensitive variant of yellow fluorescent protein (YFP) and full length RhoA.

To study RhoA activation patterns during TJ assembly, control and ZO-2 KD MDCK cells, were plated at a density of 2 x 10^5 cells on glass coverslips placed on wells with an area of 2 cm^2 within a microplate with 24 wells. 48 h later, cells were transfected with the RhoA biosensor plasmid (2 μg DNA/well) and after 24 h the monolayers were washed 5 times with PBS without Ca^{2+} and incubated in low Ca^{2+} (LC) medium (1-5 μM Ca^{2+}). After 20 h in LC medium, the monolayers were switched to normal calcium medium (1.8 mM Ca^{2+}) for different periods of time after which RhoA activation pattern were studied as the FRET/CFP ratio. To acquire and process the images we followed step by step a protocol previously published that describes in

detail the use of fluorescence resonance energy transfer biosensors [42]. The mean YFP/CFP emission ratio of entire cells was quantitated using Image J.

Immunoprecipitation

ZO-2 was immunoprecipitated from parental MDCK cells with antibodies against ZO-2 (Invitrogen, Cat. 71-1400, Camarillo, Ca) as previously described [33], with a radioimmunoprecipitation assay buffer containing: 50 mM Tris –HCl, pH 7.5, 150 mM NaCl, 1% NP-40 (vol/vol) and the protease inhibitor cocktail Complete™ (Roche Diagnostics, Cat. 11697498001, Mannheim, Germany).

Duolink *in situ* proximity ligation assay (PLA)

The Duolink *in situ* proximity ligation assay (PLA) (Olink Bioscience, Cat. 92101, Uppsala, Sweden) was done according to the manufacturer's instructions, employing a rabbit against ZO-2 antibody (Invitrogen, Cat. 71-1400; dilution 1:100; Camarillo, CA) and a mouse anti GEF-H1 antibody (Abcam, Cat. Ab90783; dilution 1:5, Cambridge, MA). After the Duolink reaction was completed, in some experiments the preparations were washed 3 times and the cell borders were stained with rat anti E-cadherin antibody (Sigma Aldrich, U3254, dilution 1:100, St. Louis, MO), followed by anti rat antibody coupled to FITC (Sigma Aldrich, F1763, dilution 1:100, St Louis, MO). Quantitative analysis of PLA assays was done using BlobFinder [43] developed by the Centre for Image Analysis at Uppsala University (www.cb.uu.se/~amin/BlobFinder/).

Cell fractionation assay

Membrane fractions from ZO-2 KD and parental MDCK cells, were isolated using the Compartmental protein extraction kit (Millipore Bioscience Research, Cat. 2145; Temecula, CA) following the manufacturer's instructions. Membrane isolates were run on a SDS-PAGE and a Western blot was performed using as plasma membrane marker, an antibody against de β1 subunit of the Na^+,K^+-ATPase (kindly donated by Michael Caplan of Yale University, New Haven, CT).

Assay to evaluate the susceptibility of cell-cell adhesion to trypsin treatment

Confluent parental and ZO-2 KD monolayers were treated with 0.05% trypsin in 0.05% EDTA at 37°C for 15 min. The enzymatic digestion was stopped by the addition of CDMEM, and the number of single cells and cell aggregates was determined in photos taken with a high resolution microscopy camera (AxioCam MRc 5, Zeiss, 0450-354, Oberkochen, Germany) placed on an inverted microscope (Zeiss Axio Observer.Z1, Oberkochen, Germany).

Cell detachment assay

Parental and ZO-2 KD cells were plated at a density of 2.5 x 10^5 cells/cm^2 in 24 well plates. After 24 h of incubation in CDMEM the cells were washed three times with PBS

and then treated for 5 or 10 min with trypsin (100 µl/well from a stock solution of 0.05% trypsin and 0.05% versene in PBS) to induce cell detachment. Then, trypsin was inactivated by the addition of CDMEM. Next, the monolayers were washed twice with PBS and fixed for 10 min with 100 µl/well of methanol. The attached cells were then stained for 5 min with filtered 1% (w/v) crystal violet at room temperature. After washing away the excess of stain with water and drying, the stained cells were solubilized in 1% (w/v) deoxycholate and 10 mM Hepes pH 7.4. The amount of stain was estimated in a plate reader at 590 nm.

Cell migration assay

Confluent monolayers grown on glass coverslips were incubated with 5 µg/ml of mitomycin C, to inhibit DNA synthesis, in order to evaluate cell migration without the interference of cell proliferation. After 2 h, the media was retired and the monolayers were wounded with the tip of a pipette. Then the monolayers were washed twice with PBS, incubated with CDMEM and placed inside an environmental chamber with the temperature controlled at 37°C (Heating Insert P Lab-TekTM S1, Zeiss, Cat. 411860-9025-000, Erbach, Germany) (TempModule S1, PeCon, Cat. 800-800 000, Erbach, Germany) and an atmosphere of 5% CO_2 (CO_2 Module S1, PeCon, Cat. 810-800 001, Erbach, Germany) (CO_2-Cover PM S1, PeCon, Cat. 411857-9110-000, Erbach, Germany) located on an inverted microscope Zeiss Axio Observer.Z1. Images were taken with a high resolution microscopy camera (AxioCam MRc 5, Zeiss, 0450-354, Oberkochen, Germany) 0, 12 and 24 h after monolayer wounding employing the Axiovision 4.0 program. To automatically analyze the wound healing assay we employed TScratch software version 1.0 (http://cse-lab.ethz.ch/software/).

Cell mobility assay

Parental and ZO-2 KD cells were plated at low density (2.5 X 10^4 cells/cm^2) and 24 h later a cell mobility analysis was performed using the inverted microscope Zeiss Axio Observer.Z1 equipped with an environmental chamber with the temperature controlled at 37°C (Heating Insert P Lab-TekTM S1, Zeiss, Cat. 411860-9025-000, Erbach, Germany) (TempModule S1, PeCon, Cat. 800-800 000, Erbach, Germany) and an atmosphere of 5% CO_2 (CO_2 Module S1, PeCon, Cat. 810-800 001, Erbach Germany) (CO_2-Cover PM S1, PeCon, Cat. 411857-9110-000, Erbach, Germany). The movement of isolated cells and of cell islets was followed by time-lapse video microscopy with a digital camera (AxioCam MRc 5, Zeiss, 0450-354, Oberkochen, Germany) recording every 4 min for 5 h at 10 X magnification. The trajectories and the migration speeds were analyzed with the Manual tracking ImageJ plugin (http://rsb.info.nih.gov/ij/plugins/track/track.html).

Cyst formation

ZO-2 KD and parental MDCK cells were trypsinized, resuspended in 30 µl of DMEM at a cell density of 3 x 10^6 cells/ml, mixed with 20 µl of Matrigel (BD Bioscience, Cat. 356234, Rockville, MD), plated on top of a Transwell insert (Polycarbonate filter, 6.5

mm diameter, 0.4 μm pores; Cat. 3414; Corning, Tewksbury, MA), placed inside a 24 multiwell plate containing DMEM, and incubated for 1 h at 37°C in an air 5% CO_2 atmosphere. Then the upper chamber of the Transwell was bathed with 100 μl of CDMEM and left in the incubator for additional 10 days. Replenishing the culture media with fresh CDMEM every third day. The cysts formed were then fixed with 2% paraformaldehyde, permeabilized with 0.5% of Triton X-100 in PBS, and processed for immunofluorescence in the Transwell insert by overnight incubation with a rabbit antibody against claudin-1 (Invitrogen, Cat. 51-9000, dilution 1:1000, Camarillo, CA) and a mouse monoclonal antibody against gp135/podocalyxin (Invitrogen, Cat. 39-3800, dilution 1:100, Camarillo, CA). The Transwell were next incubated overnight with an anti mouse antibody coupled to Alexa Fluor 488 (Life Technologies, Cat. A11001, dilution 1:300 Eugene, OR) and an anti rabbit antibody coupled to Alexa Fluor 594 (Life Technologies, Cat. A11012, dilution 1:300 Eugene, OR). After 12 washes with PBS, the Transwell inserts were inverted and the filters detached with a cutter. Then the Matrigel matrixes containing the cysts were pulled away from the underlying filters by pushing the gelatinous matrixes with a spatula and placing them upon a slide, where they were covered for 5 min. with Topro-3 (Life Technologies, Cat. T3605, Eugene, OR) dissolved in PBS (dilution 1:10,000), washed 5 times with PBS and covered with mounting media and a coverslip. Samples were observed in the Leica SP8 confocal microscope.

Quantitative Reverse Transcription-Polymerase Chain reaction (qRT-PCR)

Total RNA was extracted from parental and ZO-2 KD MDCK cells using the TRI-reagent (Sigma-Aldrich, Cat. T9424, St. Louis, MO). RT-qPCR was performed by a one-step method employing KAPA SYBR® FAST qPCR kit (KAPA Biosystems, Cat. KK4600, Wilmington, MA) according to the manufacturer's instructions. Quadruplicate samples were subjected to qPCR by using the Step One plus Real Time PCR system (Applied Biosystems Cat. 4376600, Carlsbad, CA). The PCR conditions were: after an initial cycle of 5 min at 42°C, one cycle of 5 min at 92°C and 40 cycles of amplification (30 sec at 92°C and 30 sec at 62°C) and a melt curve (15 sec at 95°C; 1 min at 60°C; 15 sec at 95°C). Primers used for amplification were as follows: claudin-2, forward: CAAGCCCTGAAGACACTTCTG, reverse: GTGCTGTAGATGTCACACTGG; claudin-4 forward: TGCACCAACTGCGTGGAGGATGAG, reverse: ACCACCAGCGGGTTGTAGAAGTCC; claudin-7, forward: CATTGTGGGAGGTCTTGCTG, reverse: AGAGTTGGGCTTAGGGTAGG; integrin β1, forward: CTCCAGCCAGAAGATATTACTCAG, reverse: AAATGAACCAAACCCAATTCGG; integrin β4, forward: AAATCCACTTCAACTGGCTG, reverse: GCACACCTTCATCTCATAGTC; large ribosomal protein P0 (PRP0), forward: TACAACCCTGAAGTGCTTGAC, reverse: GCAGATGGATCAGCCAAGAAG. The relative abundance of claudin mRNA was expressed as sample vs parental in comparison to (PRP0) mRNA and was calculated using $2^{-\Delta\Delta ct}$ method.

Measurement of transepithelial electrical resistance (TER)

Parental and ZO-2 KD MDCK cells were grown on 1.12 cm^2 polyester membranes Transwell clear inserts (pore size 0.4 μm; Corning Inc., Cat. 3460, Corning, NY). TER was continuously measured from each insert by using an automated cell monitoring system, cellZscope (nanoAnalytics GmbH, Munster, Germany). TER values were obtained by using the cellZscope software, version 1.5.0.

Paracellular flux assay

The paracellular flux assay was done as previously described [44]. Briefly 200 μl of tracer solution 10 μg/ml FITC-Dextran of 10 kDa (Invitrogen Cat. D1821, Eugene, OR) or 70 kDa (Invitrogen D1823, Eugene, OR) were added to the apical side of confluent parental and ZO-2 monolayers plated on Transwell inserts (Costar, Cat. 3470, Tewksbury, MA). After one h of incubation at 37°C, media from the upper and lower chambers were collected and the amount of FITC-Dextran was measured in a fluorometer (excitation 492 nm; emission 520 nm).

Drugs and inhibitors

C3 transferase from *Clostridium botulinum* (Cytoskeleton, Inc., Cat. CT03, Denver, CO), was prepared as 1 mg/ml stock in water, and used at a concentration of 1 μg/ml.
Y27632 (Merck KGaA, Cat 688000, Darmstadt, Germany), was prepared as a 10 mM stock in water, and used at a concentration of 10 μM.
ML-7 (Merck KGaA, Cat 475880, Darmstadt, Germany) was prepared as a 10 mM stock in DMSO, and used at a concentration of 10 μM.
Mitomycin C from *Streptomyces caespitosus* (Sigma-Aldrich, Cat. M0503, St. Louis, MO) was prepared as a 5 mg/ml stock in water, and used at a concentration of 5 μg/ml.
Forskolin (Sigma-Aldrich, Cat. F6886, St. Louis, MO) was prepared as a 10 mM stock in DMSO, and used at a concentration of 50 μM.

Results

ZO-2 KD cells display an altered cytoarchitecture accompanied by an atypical abundance of stress fibers

Treatment of MDCK monolayers with a shRNA that completely abolishes ZO-2 expression (ZO-2 KD), augments the expression of ZO-1 (Fig. 1A), increases the size of cells by hypertrophy [39] and triggers an atypical morphology characterized by areas that detach from the substrate, wider intercellular spaces and regions where some cells grow on top of others (Fig. 1B). These changes vanish upon transfection of a hZO-2 construct, not susceptible to the shRNA against ZO-2, into ZO-2 KD cells (Fig. 1 A and B). By immunofluorescence, ZO-2 KD MDCK, show in lateral images an altered apical profile, with areas where the apical surface appears to have overgrown (Fig. 1C). Next we analyzed in *en face* views the distribution of actin at the apical and basal levels. To discard the possibility that the phenotypic changes could be the result of shRNA off-target effects, we analyzed three clones of ZO-2 KD MDCK cells: clone IC5 that was

employed for the experiments depicted in Fig 1A, B, C and D and clones IC6 and 2D1 in Figure 1D. This last figure reveals that ZO-2 KD cells maintain at the apical level, a ring of actin at the cell borders, while at the basal level, they exhibit large cumulus of stress fibers. Hereafter, and unless otherwise indicated, all the ZO-2 KD cells used in this work correspond to clone IC5, and will be referred only as ZO-2 KD cells.

The absence of ZO-2 favors cells disaggregation, vinculin recruitment to focal adhesions, decreases the expression of claudin-7 and integrin β 1 and facilitates cell detachment.

Because monolayers of ZO-2 KD cells exhibit wider intercellular spaces (Fig. 1B), we next tested the susceptibility of these cells to extracellular trypsin treatment. For this end, confluent parental and ZO-2 KD cells transfected or not with hZO-2, were treated with 0.05% trypsin in 0.05% EDTA at 37°C for 15 min. Then, the dispersed cells were observed under a microscope and single cells and aggregates of two to three cells, and of more than three cells were counted. Figure 2A shows that the percentage of single cells against cell aggregates was higher in ZO-2 KD than in parental cells, and that this effect was reversed by hZO-2 transfection. These results indicate that lack of ZO-2 debilitates cell-cell adhesion.

As we observed that in ZO-2 KD cells areas of the monolayers are not attached to the substrate (Fig. 1B), we next performed a cell detachment assay by treating parental and ZO-2 KD cells transfected or not with hZO-2, for 5 or 10 min with 0.05% trypsin in 0.05% EDTA at 37°C. Figure 2B reveals that the lack of ZO-2 facilitates cell to substrate detachment, indicated by the reduced amount of cells stained with crystal violet that remain in the wells after trypsin treatment. This effect diminished upon transfection of hZO-2 to ZO-2 KD cells. Next we explored the expression of vinculin at the basal surface of ZO-2 KD cells, and observed a profusion of vinculin spots in ZO-2 KD cells that diminished upon transfection of hZO-2 (Fig. 2C). These results hence suggest, that in ZO-2 KD cells, the areas of the monolayers that still remain attached to the substrate, reinforce their focal adhesions with vinculin and stress fibers.

Then, with the aim of understanding the enhanced cell to substrate detachment induced by the lack of ZO-2, we explored the expression of claudin-7 and integrin β 1. Claudin-7 co-localizes and forms a stable complex with integrin β 1 and its deletion leads to a reduction in integrin β 1 expression and a decreased cell-matrix adhesion [45] [46]. Figure 2D shows by Western blot (left) and immunofluorescence (right) a significant decrease in claudin-7 in ZO-2 KD cells and in addition, the Western blot shows that the amount of claudin-7 recovers upon transfection of hZO-2 into ZO-2 KD cells. This change appears to be due to loss of protein and not to altered transcription since qRT-PCR reveals no difference in mRNA for claudin-7 between parental and ZO-2 KD cells (Figure 2E). This change is accompanied by a decreased expression of integrin β 1 in ZO-2 KD cells at the protein level, that can be reversed by hZO-2 transfection (Fig. 2F) and not by alterations in mRNA as determined by qRT-PCR (Fig. 2G).

Taken together our results suggest that the decreased expression of claudin-7 and integrin β 1 enhance the detachment of ZO-2 KD cells from the substrate.

The absence of ZO-2 triggers Rac activation and cofilin dephosphorylation that induces the formation of multiple lamellipodia and reduces directionality persistence, but increases wound closure.

Next, we explored if the absence of ZO-2 altered the formation of lamellae. We found that ZO-2 KD monolayers, wounded 24 h earlier with a pipette tip form bigger lamellae than parental cells and this effect is reversed when ZO-2 KD cells are transfected with hZO-2 (Fig. 3A). Figure 3B reveals that individual MDCK ZO-2 KD cells and islands display many lamellae that protrude from multiple points around the cells, while individual parental cells and islands protrude a single lamella.

Because integrin $\alpha_6\beta_4$, a receptor of laminin, mediates the formation and stabilization of lamellae [47], we analyzed the expression of integrin β 4, finding that the amount of this protein increased in ZO-2 KD cells, and diminished upon transfection of hZO-2 into ZO-2 KD cells (Fig. 3C), while no change was detected at the mRNA level with a qRT-PCR (Fig. 3D).

Then, we analyzed the phosphorylation status of cofilin in parental and ZO-2 KD MDCK cells, since F-actin binding, severing and depolymerization activity of cofilin is activated by its dephosphorylation at serine 3. Cofilin activity is crucial for the formation of lamellipodial protrusions and cell motility, as the actin monomers disassembled from the rear of the network, are recycled to the leading edge for further rounds of polymerization (for review see [48]. Figure 3E shows that in ZO-2 KD cells cofilin is significantly less phosphorylated than in parental cells, thus suggesting that the profusion of lamellae triggered by the absence of ZO-2, is mediated by an increased cofilin activity.

Next we analyzed Rac1 activity, since this member of the Rho family of GTPases promotes cofilin dephosphorylation [49]. Figure 4A reveals in a pulldown assay, that a higher amount of active, GTP-bound Rac1, is present in ZO-2 KD cells in comparison to parental cells, and this increase returns to its basal level upon transfection of hZO-2 into ZO-2 KD cells. These results hence suggest that activation of cofilin in ZO-2 KD cells might be mediated by Rac1.

Rac is known to promote the formation of lamellae and random cell migration, instead of directional migration [50]. Hence, we followed by time-lapse video microscopy the movement of isolated cells and of cells within islets from ZO-2 KD and parental cultures. Figure 4B, shows examples of trajectories followed by parental and ZO-2 KD single cells and islands. We observed that ZO-2 KD cells travel a longer distance than parental cells, and that in both cases islands of cells travel longer distances than isolated cells (Individual cells: parental, 55.7 ± 7.4 μ m, n=20 cells vs ZO-2 KD, 74.96 ± 9.5 μ m, n=19 cells; Islands: parental, 71.02 ± 6.8 μ m, n=21 cells vs ZO-2 KD, 139.4 ± 4.8 μ m, n=19 cells). Then, we determined the directionality index, calculated as the ratio of the distance between starting and ending points divided by the actual trajectory [51] and found a lower directionality index in ZO-2 KD cells (Fig. 4C). These results hence indicate that ZO-2 KD cells are moving more than parental cells, but that the appearance in ZO-2 KD cells of multiple lamellae that are competing for movement of the cell/island reduces the directionality persistence of these cells.

Next, we tested if the absence of ZO-2 affects wound closure. For this purpose confluent monolayers of parental and ZO-2 KD cells transfected or not with hZO-2, were treated for 2 h with mitomycin-C to prevent proliferation during migration. Then the monolayers were scratched with a pipette tip and the degree of wound closure was evaluated 7 and 14 h later. Figure 4D reveals that wound closure is more efficient in ZO-2 KD than in parental cells. Upon transfection of hZO-2 into ZO-2 KD cells we do not observe a significant effect by the 7th h, but at the 14th h a diminished wound healing is detected in comparison to ZO-2 KD cells, thus indicating that wound closure is modulated by ZO-2.

Loss of ZO-2 triggers the activation of RhoA and its downstream effector ROCK II

Previously it was demonstrated that a dominant active RhoA, another member of the Rho family of GTPases, regulates epithelial intercellular junctions, produces aggregates of stress fibers at the basal membrane and generates areas of multilayers within the monolayer [52]. Moreover, it was reported that an increase in active RhoA level triggered by the expression of p114RhoGEF, induced in corneal epithelial cells the development of apical elongations with a dome-like appearance [53]. Since these observations resemble the changes we observe in ZO-2 KD cells (Fig. 1), we next explored whether the absence of ZO-2 had an impact on RhoA activation.

Figure 5A shows through a G-LISA™ assay, that a higher amount of active RhoA is present in ZO-2 KD cells than in parental cells. To explore in more detail the activation of RhoA, we next performed a RhoA GTPase activation assay that detects the interaction of RhoA with a fusion protein that contains the RBD domain of rhotekin, using a pulldown strategy. Figure 5B (first three lanes) reveals higher amount of active RhoA, relative to total Rho, in ZO-2 KD cells. Surprisingly, this figure also shows that transfection of a hZO-2 construct into parental or ZO-2 KD cells further increases RhoA activation, thus indicating that RhoA activity increases above the level present in parental cells both upon ZO-2 depletion or over-expression.

Next we explored in parental and ZO-2 KD cells, the capacity of RhoA to respond to an activator, the G-protein-coupled receptor agonist, phospholipid lysophosphatidic acid (LPA). Figure 5B shows that treatment of parental cells with LPA increases RhoA activity while the absence of ZO-2 blocks the capacity of RhoA to respond to LPA treatment. Taken together, these results suggest that in ZO-2 KD cells the activity of RhoA is higher than in parental cells, but cannot be stimulated further unless ZO-2 is restored into the cells.

Then we analyzed the impact of hZO-2 transfection on stress fiber formation in ZO-2 KD cells. We observed in the same monolayer, cells with different levels of transfection efficiency, which were labeled as high, medium and low ZO-2 expressing cells (Fig. 5C, left panel). Surprisingly, in cells with the same level of ZO-2 expression, we could find differences in the profusion of stress fibers, as in some cells the amount decreased, increased or had no change, in comparison to the surrounding untransfected cells (Fig. 5, right panel). However, the frequency of appearance of the different patterns, revealed that in 65 and 63% of cells displaying low and high over-expression of Z0-2 respectively, the amount of stress fibers diminished in comparison to the surrounding untransfected cells, while in cells with a medium over-expression

of ZO-2, 45% showed a decrease in stress fibers while 38% displayed no change (Fig. 5C, lower panel). These observations hence suggest that hZO-2 transfection into ZO-2 KD cells, changes in the majority of cells the amount of stress fibers, being a reduction in stress fiber profusion the most frequent behavior.

We next aimed to explore the activation RhoA in ZO-2 KD and parental cells during the *de novo* formation of cell-cell contacts. For this purpose we performed a Ca-switch assay, in which cells were transferred from low Ca^{2+} (LC, 1-5 μ M) to normal Ca^{2+} (NC, 1.8 mM) containing media, to induce the formation of cell-cell junctions, and evaluated at different times after the Ca-switch the spatiotemporal dynamics of RhoA activation through the use of a RhoA biosensor with intramolecular fluorescence resonance energy transfer (FRET) [41]. Figure 5D shows that in cells incubated in LC media, bigger patches of high RhoA activity are present in ZO-2 KD cells than in parental cells. Ca-switch induces the activation of RhoA, and a higher level of activity is present in ZO-2 KD versus parental cells from 0 to 60 min after the Ca-switch. These results hence indicate that before calcium mediated cell-cell adhesion is established, and early during the process of cell junction formation, the lack of ZO-2 favors the activation of RhoA.

We next studied in parental and ZO-2 KD cells transfected or not with hZO-2, the downstream effector of RhoA, the kinase ROCK. The Western blot in figure 6A, shows an increased expression of ROCK II in ZO-2 KD cells transfected or not with hZO-2 versus parental cells (right panel), while ROCK I showed no change between parental and ZO-2 KD cells (left panel). The increase in ROCK II was expected since more active RhoA was detected in ZO-2 KD cells transfected with ZO-2, than in ZO-2 KD cells. (Fig. 5B).

ROCK II induces actin-myosin contractility by phosphorylating the regulatory myosin light chain (MLC2), and accordingly, in figure 6B the Western blot reveals an increased phosphorylation of MLC2 in ZO-2KD in comparison to parental cells and a diminished phosphorylation upon transfection of hZO-2 into ZO-2 KD cells. The latter might seem surprising since the amount of active RhoA is higher after hZO-2 transfection into ZO-2 KD cells. However, the regulation of MLC2 phosphorylation is extremely complex and involves multiple MLC kinases, regulated by a variety of upstream molecules (for review see [54]), including Rac which in our hands is less active upon transfection of hZO-2 into ZO-2 KD cells (Fig. 4A).

By immunofluorescence we observe that in ZO-2 KD cells, myosin IIa and the phosphorylated MLC2 concentrate at the cumulus of stress fibers present the basal surface (Fig 6C). The nuclear staining obtained with the anti p-MLC2 antibody corresponds to a non-specific staining observed previously [55].

To confirm these results, we next analyzed the impact of C3 transferase from *Clostridium botulinum*, an ADP-ribosyl transferase that selectively ribosylates RhoA, B and C proteins rendering them inactive [56]; of Y27632, a potent, cell permeable, reversible and selective inhibitor of ROCK I and II [57]; and of ML-7 a selective inhibitor of myosin light chain kinase (MLCK) [58], an enzyme that phosphorylates MLC2. Figure 6D reveals that when ZO-2 KD cells are treated with C3 and ML-7 an increased signal of myosin IIa and p-MLC2 is detected at the apical borders of the cells. In parental cells, a similar situation is observed with myosin IIa after treatment with C3. When parental or ZO-2 KD cells are treated with C3, the profusion of actin,

myosin IIa and p-MLC2 basal stress fibers and clusters disappears, while treatment with Y27632 exerts a similar, yet less profound effect. The incubation with ML-7 elicits no significant effect on actin, myosin IIa and p-MLC2 present at the basal level. A similar effect is observed in parental cells. Altogether, these results suggest that the formation of basal stress fibers requires the activation of RhoA and ROCK, but not that of MLCK.

GEF-H1 that promotes the formation of stress fibers, is recruited by cingulin to the cell borders of ZO-2 KD cells

The activity of small G proteins is stimulated by GEFs, and in particular that of RhoA at the apical junctional complex is regulated by two: p114RhoGEF whose association to the TJ adaptor protein cingulin, promotes TJ formation and maturation [53], and GEF-H1 whose association to cingulin and paracingulin inhibits its GEF activity and reduces RhoA signaling [59] [60]. Since the absence of ZO-2 promotes RhoA activation, we explored whether ZO-2 associates to GEF-H1 in parental MDCK cells. Figure 7A shows that ZO-2 and GEF-H1 co-immunoprecipitate. Next, we made a proximity ligation assay (PLA) using a rabbit antibody to detect ZO-2 and a mouse antibody for GEF-H1. Figure 7B confirms, with the appearance of discrete red fluorescent spots, the interaction of ZO-2 and GEF-H1 in the cell borders and cytoplasm.

Then, we transfected parental MDCK cells with EGFP and an active form of GEF-H1 (GEF-H1-C53R), and observed that transfected cells exhibit abundant stress fiber at the basal level (Fig. 7C, upper row). In accordance, in ZO-2 KD cells transfected with EGFP and a dominant negative GEF-H1 (GEF-H1-Y393A) we observe a diminished amount of stress fibers (Fig. 7C, lower row). These results hence suggest that the lack of ZO-2 induces the over-abundance of stress fibers through a process mediated by GEF-H1.

Previously it was demonstrated that p21-activated-kinase 4 (PAK4) mediates the phosphorylation of GEF-H1 at the serine residue located within the RRXSLXG consensus site. This phosphorylation acts as a switch to block GEF-H1-dependent stress fiber formation [61]. Because we observe a profusion of stress fibers in ZO-2 KD cells, we next explored the phosphorylation status of GEF-H1 in these cells. Figure 7D shows a higher content of phospho-GEF-H1 (p-GEF-H1) in parental than in ZO-2 KD cells, thus indicating that the formation of stress fibers induced by ZO-2 absence, involves GEF-H1 dephosphorylation. Instead, the amount of total GEF-H1 is not affected by the lack of ZO-2.

Next we studied whether the distribution of GEF-H1 is altered in ZO-2 KD cells in comparison to parental MDCK. By immunofluorescence we observed that in parental MDCK cells, GEF-H1 localized at the cell borders and Golgi, as previously reported [62] [61], and that the absence of ZO-2 increased the signal of GEF-H1 at the cell borders, and disappeared the staining at the Golgi (Fig. 7E). Then, we performed a cell fractionation assay and by Western blot confirmed a higher accumulation of GEF-H1 at the plasma membrane of ZO-2 KD cells in comparison to parental cells (Fig.7F).

We asked how was GEF-H1 being recruited to the cell borders in the absence of ZO-2. For this purpose we analyzed the level of expression of paracingulin and

cingulin in ZO-2 KD MDCK cells. Figure 8A shows by immunofluorescence no apparent change in cingulin expression at the cell borders, while ZO-2 KD cells expressed paracingulin in a less intense manner than parental cells. By Western blot we observed in ZO-2 KD cells a decrease in paracingulin, accompanied by an increase in cingulin expression (Fig. 8B). The latter can be reversed by transfection of hZO-2 into ZO-2 KD cells (Fig. 8F). Then we tested if the absence of ZO-2, favored the association of cingulin to GEF-H1. Figure 8C shows in a PLA assay, that in ZO-2 KD cells in comparison to parental cells, a significantly higher amount of red spots are present, thus suggesting an increase in cingulin-GEF-H1 interaction. It is also noteworthy, that many of these positive spots are located along the cell borders (arrow).

Altogether, these results suggest that the absence of ZO-2 favors the recruitment of GEF-H1 to the cell borders by cingulin. There, the reduced expression of paracingulin might not be able to turn off GEF-H1 signaling, producing in consequence the increased RhoA signaling.

The absence of ZO-2 decreases cingulin phosphorylation and microtubules association to TJ.

Cingulin phosphorylation by adenosine monophosphate-activated protein kinase (AMPK) has recently been shown to promote microtubule association with TJ [63]. Since we had observed that the lack of ZO-2 increased the amount of cingulin, we next tested if ZO-2 KD cells displayed a change in microtubule organization at the TJ. Figure 8D reveals that ZO-2 KD cells lose the microtubules that in parental cells are aligned laterally to TJs, forming a non-centrosomal network organized into a planar apical structure. However, treatment of ZO-2 KD cells with forskolin, an inducer of AMPK activation [64] as well as the reintroduction of ZO-2, triggered the reappearance of microtubules at the cell borders

To analyze the effect of these treatments on cingulin phosphorylation, we performed a mobility shift detection assay for cingulin, running the extracts of parental and ZO-2 KD cells on phosphate-affinity SDS-PAGE with a dinuclear manganese complex of acrylamide-pendant Phos-tag, which binds and retards the migration of phosphorylated proteins. In figure 8E we observe a higher migration of cingulin in ZO-2 KD cells in comparison to parental cells that is reversed by hZO-2 transfection or forskolin. Then we analyzed if ZO-2 modulates the interaction of cingulin with β-tubulin. Figure 8F reveals that the amount of β-tubulin that co-immunoprecipitates with cingulin diminishes in ZO-2 KD cells in comparison to parental cells, and that this effect is reversed upon hZO-2 transfection or treatment with forskolin.

Altogether these results suggest that ZO-2 facilitates the phosphorylation of cingulin by AMPK, which allows the interaction of cingulin with microtubules at the apical junctional region.

ZO-2 regulates TJ barrier function and claudin-2 expression

We next analyzed the development of the TJ barrier function in ZO-2 KD and parental monolayers during the Ca-switch. Figure 9 A shows that ZO-2 KD cells reach a much

lower peak TER value than parental cells. This effect is due to the lack of ZO-2, as it can be reversed by the transfection of hZO-2 (Figure 9A).

We also observed that when TER is stable in both cell lines (e.g. 40 h after the Ca-switch), the value in ZO-2 KD cells is 43% higher than in parental cells (Figure 9A, inset), and the paracellular permeability of the monolayers to fluorescent dextran of 10 and 70 kDa is lower in ZO-2 KD than in parental cells (Figure 9B). These effects are due to the absence of ZO-2 as the transfection of hZO-2 into ZO-2 KD cells decreases TER and augments dextran permeability at steady state.

It is well established that the set of claudins expressed by a tissue defines the selectivity and "tightness" of the paracellular pathway (for review see [21]. Claudin-2 is a key determinant of TJ ionic selectivity, as it forms paracellular cationic pores [65, 66] that increase TJ permeability [67] and decrease TER [68]. Instead, claudin 4 has been shown to exert the opposite effect and to function as a cationic barrier [69] or an anion pore [70]. With this in mind, we next analyzed the expression of claudins -2 and -4 in parental and ZO-2 KD cells.

By immunofluorescence claudin-2 is not detected at the cell-cell junctions in ZO-2 KD cells at any time after the Ca-switch (Fig. 9C), while at the cell borders of parental cells, it is barely present at the peak of TER and conspicuously found at steady state. In contrast, claudin-4 is present in both parental and ZO-2 KD cells, however at the steady state, it is more abundant at the cell borders of MDCK ZO-2 KD cells than in parental cells.

The Western blot confirms that a higher amount of claudin-2 is present in MDCK parental cells in comparison ZO-2 KD cells (Fig. 9D, left). Since the transcription factor GATA-4 controls claudin-2 expression [71], we next analyzed the expression level of GATA-4 in ZO-2 KD cells. The Western blot in figure 9E shows the same level of expression of GATA-4 in ZO-2 KD in comparison to parental MDCK cells. However, upon transfection of GATA-4 to ZO-2 KD cells, we observe a significant increase of claudin-2 expression. Then, by qRT-PCR we analyzed the mRNA level for claudin-2 and detected no differences between parental and ZO-2 KD cells (Fig. 9F, left). These results hence indicate that the decreased expression of claudin-2 in ZO-2 KD cells is regulated post transcription.

The Western blot of claudin-4 reveals an increased expression of this protein in ZO-2 KD cells (Fig. 9D, right). In agreement, the qRT-PCR reveals a similar increase of claudin-4 mRNA in ZO-2 KD cells (Fig. 9F right) thus indicating that the lack of ZO-2 up-regulates at the transcriptional level the expression of claudin-4.

Altogether, our results suggest that the increased TER detected at steady state in the absence of ZO-2, is due to the generation of an altered expression of claudins.

The lack of ZO-2 triggers Cdc42 activation, mitotic spindle disorientation and the formation of cysts with multiple lumens

In ZO-2 KD cells, some cells are located on top of others (Fig. 1B). This observation prompted us to explore whether the lack of ZO-2 triggers an alteration in the orientation of the mitotic spindle angle. Figures 10A and B show that in parental cells, 56% of divisions occur parallel to the substrate surface (0-10^{o} angle) while in ZO-2 KD cells, 34% of the mitotic spindles are parallel to the surface of the substrate. Next, we

tested whether the disorientation of the mitotic spindle, could be reversed by blocking the RhoA/ROCK/MLC2 signaling pathway. The radial histograms in figure 10B show that treatment with C3, Y27632 or ML-7 decreases the percentage of ZO-2 KD cells in metaphase with a 0-10^{o} angle, to 17%, 29% and 25% respectively. These results hence indicate that the lack of ZO-2 triggers the disorientation of the mitotic spindle, through a mechanism sensible to a precise amount of active RhoA within the cell, as both the over-activity of RhoA present in ZO-2 KD cells as well as the inhibition of RhoA with C3 or of its downstream elements ROCK and p-MLC2, trigger the same effect.

Next we tested whether the lack of ZO-2 affects the development of cysts in three-dimensional (3D) cultures that resemble more closely the physiological condition. For this purpose we cultured ZO-2 KD and parental MDCK cells in the extracellular matrix Matrigel. Figure 10C shows that in ZO-2 KD cells 60% of cysts have multiple lumens, while 81% of cysts from parental cells display one hollow lumen surrounded by one layer of polarized cells. These results hence indicate that the lack of ZO-2 severely disrupts epithelial morphogenesis.

Dominant negative or constitutively activated Cdc42 inhibit centrosome polarization [72], and Cdc42 depletion induces misoriented cell division that leads to the formation of cysts with multiple lumens [73]. This prompted us to explore the activity of Cdc42 in ZO-2 KD cells in a pulldown assay. Figure 10D reveals that a higher amount of active, GTP-bound Cdc42, is present in ZO-2 KD cells in comparison to parental cells. Hence, our results suggest that the disorientation of the mitotic spindle that triggers the formation of multiple cysts is a response to the increased activity of RhoA and Cdc42 triggered by the lack of ZO-2.

Discussion

Here we have found that ZO-2 is a key player in the regulation of Rho, Rac and Cdc42 proteins, which are critical for the proper development of cell architecture and TJ sealing (Fig. 11).

We show that ZO-2 KD cells exhibit large clusters of stress fibers, in agreement to a similar finding observed in human dermal microvascular endothelial cells upon ZO-1 depletion [74]. This is in contrast to ZO-1/-2 depleted cells that do not show a profusion of stress fibers and instead display a more linear cell border profile [75]. We also observed that ZO-2 KD MDCK, have an altered apical profile, where the apical surface appears to have overgrown. We suggest that this profile change might be due to contraction of perijunctional F-actin, as it occurs in human corneal epithelial cells upon expression of p114RhoGEF [53]. However this point requires further analyses.

To explore if ZO-2 KD cells have debilitated cell-cell adhesions that could explain the observed wider intercellular spaces, we tested their susceptibility to extracellular trypsin, finding that it was higher in ZO-2 KD than in parental cells. These results are similar to those obtained with ZO-1 knock-out/ZO-2 KD Eph4 cells [76].

We also observed in ZO-2 KD cells, areas of the monolayers that are not attached to the substrate and an increased response in a cell to substrate detachment

assay that might be explained by the reduction in claudin-7 and integrin $\beta 1$, that favor cell substrate adhesion [45, 46]. The overexpression of vinculin at the basal surface of ZO-2 KD cells was expected because the elevated phosphorylation of MLC2 found in ZO-2 KD cells is indicative of actomyosin contraction, which is known to recruit vinculin to focal adhesions [77].

In ZO-2 KD cells, cofilin is dephosphorylated, multiple lamellipodia protrude from the cells and directional migration decreases. Cofilin phosphorylation can be upregulated by RhoA activity, since LIM kinases (LIMK) phosphorylate cofilin at serine 3 [74], and these kinases are in turn, activated by ROCK phosphorylation [75]. However, the decreased phosphorylation of cofilin observed in ZO-2 KD cells, might be explained by the increased Rac activity that promotes the activation of cofilin phosphatases [49] and lamellipodia formation [78]. In addition, we have observed that ZO-2 KD cells exhibit an increased transcriptional activity of YAP (Yes associated protein) [39] that promotes the expression of miR-29 that specifically inhibits the translation of phosphate and tensin homolog (PTEN) [79] and the transcription of Pik3cb, a gene that encodes for the catalytic subunit p110 of PI3K [80] Thus YAP transcriptional activity leads to a decreased expression of PTEN and higher amount of PIP3 in ZO-2 KD cells in comparison to parental cells [39]. This is important since Slingshot-1L, a cofilin specific phosphatase, is activated by phosphoinositide 3 kinase (PI3K) [81]. Hence, the decreased phosphorylation of cofilin found in ZO-2 KD cells might be the result of both an increase in the activity of Rac and Slingshot-1L.

With respect to the wound-healing assay, the results were expected since longer distances were travelled by islands of MDCK ZO-2 KD cells, than by parental cells. These results are in agreement with the observation that in human lung cancer cells, ZO-2 inhibition increased the migration rate [82]. Moreover, the reduced directional migration in cells lacking ZO-2, is consistent with the observation that high Rac activity induces random cell migration [50]. Taken together, our observations suggest that the lack of ZO-2 triggers Rac and cofilin activation that induces a reorganization of the actin cytoskeleton manifested by the appearance of multiple lamellipodia and non-directional cell migration.

The apparent contradictory observation that ZO-2 KD cells exhibit a reduced directional persistence while at the same time show a more effective wound closure, can be explained by considering that a reduced directional migration, has a low impact in a wound closure assay, since in this case the migrating cells are surrounded by other cells and hence can only migrate into the direction of the wound. Therefore in this condition the greater mobility triggered by the lack of ZO-2, favors wound closure.

Since the activation of the Rho protein family with *Escherichia coli* cytotoxic necrotizing factor 1 (CNF-1) [83], or the expression of a dominant active RhoA, produce aggregates of stress fibers at the basal membrane [52, 84], we explored whether the absence of ZO-2 had an impact on RhoA. This quest was reinforced by a recent observation showing that the junctional adhesion molecule-A (JAM-A) binds to ZO-2, which in turn, through its association with afadin and PDZ-GEF1, recruits and activates the small GTPase Rap2c that negatively control the contraction of the apical cytoskeleton by RhoA [7].

By ELISA and pulldown assays we showed that in sparse cultures, RhoA is more active in ZO-2 KD cells than in parental cells. With the RhoA biosensor, we further showed that the absence of ZO-2 induced the activation of RhoA before calcium mediated cell-cell adhesion is established, and early during the process of cell junction formation.

Then we analyzed the expression of ROCK I and ROCK II finding that in MDCK ZO-2 KD cells only the expression of the latter increases. In agreement it was previously found that ROCK II and not ROCK I, mediates the disassembly of the apical junctional complex in epithelial cells [85] and partially localizes in stress fibers [86].

To further confirm that the profusion of stress fibers in MDCK ZO-2 KD cells is due to the activation of the RhoA/ROCK signaling pathway, we treated the monolayers with inhibitors of Rho and ROCK and observed that the clusters of stress fibers disappeared. Instead, treatment with ML-7 an inhibitor of MLCK [58], which phosphorylates MLC2, had no effect on the amount of stress fibers, thus indicating that the lack of ZO-2 triggers the formation of basal stress fibers through the activation of RhoA and ROCK, but not of MLCK.

In ZO-2 KD cells the reduced expression of paracingulin, that down-regulates GEF-H1 activity [60], might result in RhoA activation and the subsequent formation of stress fibers. The latter was confirmed observing that in MDCK ZO-2 KD, the transfection of an inactive form of GEF-H1, eliminates the profusion of stress fibers, and by observing that in ZO-2 KD cells, GEF-H1 is less phosphorylated at Ser886, a phosphorylation known to blocks stress fiber formation [61]. In addition, we observed that the lack of ZO-2 reduces cingulin phosphorylation mediated by AMPK, which was previously shown to be critical for the interaction of cingulin with microtubules at the apical junctional region [63].

As previously observed, here we show that MDCK cells exhibit an initial rapid increase in TER followed by a decrease to a stable level [87, 88]. However we show that the lack of ZO-2 induces a much lower peak TER value. This decrease in peak TER was previously observed when ZO-2 was partially silenced with a siRNA [38], in ZO-1 KD cells, occludin KD cells and α-catenin KD cells [89], as well as in paracingulin KD cells [60]. In addition we showed that when TER reaches a steady state, the values are 43% higher in MDCK ZO-2 KD cells, while the paracellular permeability to dextran diminishes. These effects are due to the absence of ZO-2 as they were reversed by ZO-2 transfection. Similar results were previously obtained when ZO-1 was silenced in MDCK cells [37]. The increase in TER present in ZO-2 KD cells might respond in part to the increase in size observed in these cells in comparison to parental cells [39], since the amount of current that crosses the paracellular pathway depends on both resistance of this route and on how much pathway is available per epithelial surface, and the latter depends on the size of the cells in the epithelium (for review see [90]. Now, the higher resistance of the paracellular pathway of ZO-2 KD cells might be due to the absence of claudin-2, a protein that forms paracellular cationic pores [65, 66], and the abundant expression of claudin-4 that functions as a cationic barrier [69]. Similar observations have been found as a result of silencing of IQGAP1 in MDCK cells [91].

Previously it had been shown that cingulin KD [92] and paracingulin KD [60] increased RhoA activity and claudin-2 mRNA level, while the expression of claudin-2

decreased when cingulin and paracingulin were both silenced [71, 93]. In addition, the expression claudin-2 mRNA correlated with the presence of GATA-4 transcription factor [71]. Instead, in ZO-2 KD cells we observed a decreased expression of claudin-2 not accompanied by a change in the level of mRNA for claudin-2 and the protein level of GATA-4. Hence, these results indicate that the lack of ZO-2 exert a post transcriptional negative effect on claudin-2.

As MDCK ZO-2 KD cells grow on top of each other, we explored whether this could be due to the depolarization of the mitotic spindle. We found that 66% of the mitotic spindles of ZO-2 KD cells are disoriented, and that inhibitors of RhoA, ROCK and MLC2 cannot reverse this effect and even increase the percentage of disorientation. Since similar effects have been found in cells transfected with a constitutively active RhoA [94], we conclude that the depolarization of the mitotic spindle in ZO-2 KD cells, is due to the increased activity of RhoA triggered by the lack of ZO-2. In addition, we found over activation of Cdc42 in ZO-2 KD cells, and constitutively activated Cdc42 has been found to inhibit centrosome polarization [72]. Furthermore, previous observations have shown that ZO-2 KD cells have increased phosphorylation of GSK-3 β at Ser-9 [39], which can be induced by PKC ζ under the activation of Cdc42 [95]. Therefore, our results suggest that the disorientation of the mitotic spindle that might be responsible for the formation of multiple cysts in ZO-2 KD cells is a response to the increased activity of RhoA and Cdc42. In MDCK cells we have also observed formation of cysts with multiple lumens when MDCK cells are transfected with a ZO-2 construct with a mutation in a Yin-Yang site that regulates the entry of ZO-2 into the nucleus and the phosphorylation of the protein in mature TJs [33]. Others instead, have found that MDCK ZO-1 KD cells but not ZO-2 KD cells, form cysts with multiple lumens [89].

ZO-2 is a multidomain protein involved in a vast array of activities including TJ formation, cell proliferation, regulation of gene expression [for review see [96]] and cell size [39]. This work now broadens this view showing that ZO-2 acts as a central hub that modulates the activity of Rho proteins and epithelial cytoarchitecture.

Acknowledgments

This work was supported by grant 237241 of the Mexican National Council of Science and Technology (Conacyt) to L.G.M. and 152434 to J.V.P.. A.R.S, A.D.C. and A.C.K., were recipients of doctoral fellowships from Conacyt (233193, 233211, 444536).

Figure Legends

Figure 1. The absence of ZO-2 alters the cytoarchitecture and the distribution of F-actin in epithelial MDCK cells. A) In ZO-2 KD cells no ZO-2 signal is observed by immunofluorescence (upper panel) and Western blot (lower panel). ZO-1 expression increases in ZO-2 KD cells and transfection of hZO-2 into ZO-2 KD cells reduces the amount of ZO-1 to a level similar to that in parental cells (lower panel). In the Western blot, tubulin was used as loading control. Bar = 40 μm. Statistical analysis done with One-Way ANOVA followed by Bonferroni´s post test, ***p<0.001, **p<0.01, *p<0.05. B) ZO-2 KD cells have an altered cytoarchitecture. Light microscopy images of semithin sections, show in ZO-2 KD cells of clone IC5, areas of the monolayer that have detached from the substrate (arrow), cells that grow on top of others (*) and widened intercellular spaces (arrowhead). These features are not observed in control monolayers or in ZO-2 KD cell monolayers transfected with hZO-2. Bar = 20 μm. C) The profile of ZO-2 KD monolayers of clone IC5, reveals regions where the apical surface protrudes. Lateral views of the apical surface of control and ZO-2 KD monolayers, observed by immunofluorescence, in cells stained with an antibody against gp135/podocalyxin. * Indicate apical protrusions. Bar = 20 μm. D) An apical ring of actin is detected in parental MDCK cells and ZO-2 KD cells of clones IC5, IC6 and 2D1; at the basal level the three clones of ZO-2 KD cells show a profussion of stress fibers (arrowheads), bar = 40 μm.

Figure 2. The lack of ZO-2 induces recruitment of vinculin to focal adhesions and diminishes claudin-7 and integrin β1 expression. A) Cell-cell adhesion is more susceptible to trypsin treatment in ZO-2 KD cells. Left, phase-contrast image of parental and ZO-2 KD cells transfected or not with hZO-2, and treated with 0.05% trypsin in 0.05% EDTA at 37°C for 15 min, bar = 40 μm. Right, statistical analysis done with One-Way ANOVA followed by Bonferroni´s post test, ***p<0.001. B) ZO-2 KD cells detach from the substrate in higher amounts than parental cells or ZO-2 KD cells transfected with hZO-2, after being treated for 5 or 10 min with 0.05% trypsin in 0.05% EDTA at 37°C. The attached cells were fixed with methanol and stained with crystal violet and the amount of stain was determined at 590 nm. Representative image (upper panel), quantitative analysis (lower panel). Statistical analysis done with Two-Way ANOVA followed by Bonferroni´s post test ***p<0.001. C) More abundant vinculin focal adhesion spots are present in ZO-2 KD cells than in parental cells or in ZO-2 KD cells transfected with hZO-2 (circumscribed by dotted line). Basal section images obtained with an antibody against vinculin and rhodaminated phalloidin. Bar = 40 μm D) ZO-2 KD cells have a lower amount of claudin-7 (Cl-7) than parental cells or ZO-2 KD cells transfected with hZO-2. Left upper panel, representative Western blot; left lower panel, densitometric analysis. Statistical analysis done with One-Way ANOVA followed by Bonferroni´s post test, ***p<0.001. Right panel, immunofluorescence detection of claudin-7 in parental and ZO-2 KD MDCK cells. Bar = 40 μm. E) qRT-PCR of claudin-7 from parental and ZO-2 KD cells. Statistical analysis done with Student's *t* test with Welch's correction. F) MDCK ZO-2 KD cells have a lower amount of integrin β1 than parental cells or ZO-2 KD cells transfected with hZO-2. Left, representative Western blot; right, densitometric

analysis. Statistical analysis done with One-Way ANOVA followed by Bonferroni´s post test **p<0.01. G) qRT-PCR of integrin β1 from parental and ZO-2 KD cells. Statistical analysis done with Student's *t* test with Welch's correction.

Figure 3. In ZO-2 KD cells, cofilin is dephosphorylated at Ser3 and multiple lamellae protrude from various points around the cell. A and B) The lack of ZO-2 triggers the formation of multiple lamellae. Upper panels, representative images of lamellae (arrows) in wounded monolayers (A) of parental and ZO-2 KD cells transfected (circumscribed by dotted line) or not with hZO-2, and in individual cells and cell islands (B) derived from MDCK parental and ZO-2 KD cultures. Cells were stained with rhodaminated phalloidin and DAPI to respectively detect the lamellae (arrows) in A and B, and the nuclei in B. Lower panels, corresponding quantitative analysis of the area of the lamellae determined with Image J. A) Statistical analysis done with One-Way ANOVA followed by Bonferroni's post test *p<0.05; ***p<0.001 B) Statistical analysis done with Student's *t* test. **p=0.0046; ***p<0.0001. Bars = 40 μm. In A the number of cells analyzed is the following: parental, 272; ZO-2 KD, 112; and ZO-2 KD + hZO-2, 15. In B, 31 isolated cells and 19 islands of parental cells were analyzed; while 26 isolated cells and 18 islands of ZO-KD cells were studied. These isolated cells and islands were obtained from two independent experiments. C) MDCK ZO-2 KD cells express a higher amount of integrin β4 than parental cells or ZO-2 KD cells transfected with hZO-2. Left panel, representative Western blot; right panel, densitometric analysis. Statistical analysis done with One-Way ANOVA followed by Bonferroni´s post test, **p<0.01. Results of 3 independent experiments. D) qRT-PCR amplification of integrin β4 from parental and ZO-2 KD cells. Statistical analysis done with Student's *t* test with Welch's correction. E) In MDCK ZO-2 KD cells, the phosphorylation of cofilin at Ser3 is significantly reduced in comparison to parental cells. Transfection of hZO-2 into ZO-2 KD cells increases cofilin phosphorylation. Statistical analysis done with One-Way ANOVA, followed by Bonferroni's post test, *p< 0.05; ***p<0.001. Results from two independent experiments.

Figure 4. The absence of ZO-2 activates Rac1, decreases directional migration and accelerates wound healing. A) In comparison to parental cells, the amount of active Rac1 increases in ZO-2 KD cells, and this effect is reversed by hZO-2 transfection. The active form of Rac (Rac-GTP) was isolated from parental and ZO-2 KD cells lysates, in a pulldown assay with GST-PAK-CRIB beads. Total cell lysates and pull-downs were resolved on SDS-PAGE gels and analyzed by immunoblotting for Rac1. Left, representative blot; right, relative fold increase of Rac activation quantitated by densitometric analysis of 3 independent experiments. Statistical analysis with One-Way ANOVA followed by Bonferroni's post test, *p<0.05. Dotted vertical line, indicates the place where the membrane was cut. B) Parental and ZO-2 KD cells were plated at low density and the movement of isolated cells and of cell within islands was followed by time-lapse video microscopy. Upper panels, trajectories followed by 5 representative individual cells or cells within islands. C) Directional persistence of parental and ZO-2 KD cells present as isolated cells or within islands, corresponds to distance between starting and ending points/actual trajectory. n= number of cells analyzed. Statistical analysis done with Student's t test.

**p<0.01. D) Monolayer wounding assay. Confluent monolayers of parental and ZO-2 KD cells transfected or not with hZO-2, were grown on a glass coverslip and treated for 2 h with mitomycin C, wounded with the tip of a pipette and placed under the microscope inside a chamber with the temperature controlled at 37°C and an atmosphere of 5% CO_2. Images were taken 0, 7 and 14 h after monolayer wounding. Dashed lines outline wound edges. Upper panel, representative images of clear field microscopy; lower panel, quantitative analysis done with TScratch software. Bar = 150 µm. Statistical analysis done with One-Way ANOVA followed by Bonferroni´s post test, ***p<0.001; ns, non significant

Figure 5. The absence of ZO-2 induces RhoA activation. A) In ZO-2 KD cells the activity of RhoA is higher than in parental MDCK cells. RhoA activation was measured by a G-LISA™ assay in lysates derived from ZO-2 KD and parental cells. Absorbance was read at 490 nm. Results from 6 independent experiments. Statistical analysis done with Student's *t*-test, **p=0.0014. B) RhoA GTPase activation assay done in parental, ZO-2 KD cells and ZO-2 KD cells transfected with hZO-2, using a pulldown with a fusion protein containing the RBD domain of rhotekin. Note that transfection of ZO-2 into ZO-2 KD cells increases RhoA activation above that found in ZO-2 KD cells, while the capacity of RhoA to respond to the activator LPA is lost in ZO-2 KD cells. Blot revealed with antibodies against ZO-2 and RhoA. Upper panel, representative blot; histograms 1-6, densitometric analysis of at least three independent experiments. Statistical analysis of histograms 1 and 2 was done with One-Way ANOVA followed by Newman-Keuls test, *p<0.05; ***p<0.001; of histograms 3 and 6 was done with a Student's *t* test with Welch's correction, **p<0.009; and of histograms 4 and 5 was done with a Student's *t* test, *p<0.05. C) A reduction in stress fibers or no changes in the pattern constitute the most frequent outcomes after hZO-2 transfection into ZO-2 KD cells. Cells were transfected with hZO-2 and one day later the expression of ZO-2 and F-actin was observed after incubation with antibodies against ZO-2 (green) and rhodaminated phalloidin (red). ZO-2 KD cells transfected with hZO-2 were classified as: H, high expressing; M, medium expressing and L, low expressing. Dashed line, delineates hZO-2 transfected cells; n, number of cells analyzed; left panel bar = 50 µm; right panel bar = 25 µm. D) The spatiotemporal activation of RhoA triggered by a Ca-switch assay is more pronounced in ZO-KD than in parental MDCK cells. Cells plated on glass coverslips were transfected with the RhoA biosensor and after 24 h were incubated in LC medium for 20 h. Then, the monolayers were switched to NC medium for different periods of time after which RhoA activation patterns were determined as the FRET/CFP ratio. Upper panel, representative color-coded images of three independent experiments, where cold and hot colors respectively indicate low and high levels of RhoA activity. Lower panel, graphic representation of the mean FRET/CFP ratio for entire cells. n, number of cells evaluated.

Figure 6. In ZO-2 KD cells the Rho/ROCK II/MLC2 pathway is more active than in parental cells. A) In MDCK cells, the amount of ROCK II increases in accordance to the amount of active RhoA present in parental and ZO-2 KD cells transfected or not with hZO-2. Lysates derived from confluent parental and ZO-2 KD cells transfected or not with hZO-2, were employed for Western blotting with specific antibodies against

ROCK I and ROCK II. The upper panels show representative images and the lower panels the corresponding quantitative analysis. Results from at least four independent experiments. Statistical analysis for ROCK I was done with Student's *t* test. ns, non significant. Statistical analysis for ROCK II was done with One-Way ANOVA followed by Bonferroni´s post test, ***p<0.001; **p<0.01. B) ZO-2 KD cells have a higher amount of phosphorylated MLC2 (p-MLC2) than parental cells. Lysates derived from confluent parental and ZO-2 KD cells transfected or not with hZO-2, were employed for a Western blot done with a specific antibody against p-MLC2 at Ser20. The upper panel shows a representative image and the lower panel the corresponding quantitative analysis. Results from 5 independent experiments. Statistical analysis done with One-Way ANOVA followed by Bonferroni´s post test, ***p<0.001; *p<0.05. C) In ZO-2 KD cells, myosin IIa (Myo IIa) and p-MLC2 are present at the large cumulus of stress fibers found at the basal surface (arrows). ZO-2 KD and parental cells were treated for immunofluorescence with specific antibodies against myosin IIa and p-MLC2 at Ser20. Bar = 40 μm. D) In ZO-2 KD cells, the inhibition of RhoA with C3 transferase and of ROCK with Y27632 diminishes the appearance at the basal cellular level of F-actin-myosin stress fibers and clusters, while the inhibition of MLCK with ML-7 elicits no significant change at the basal level. Bar = 40 μm.

Figure 7. GEF-H1 mediates the formation of stress fibers in ZO-2 KD cells. A) ZO-2 and GEF-H1 co-immunoprecipitate. ZO-2 was immunoprecipitated, run on SDS-PAGE, and blotted against GEF-H1. B) ZO-2 and GEF-H1 interact. Proximity ligation assay (PLA) done with a rabbit antibody against ZO-2 and a mouse antibody against GEF-H1. Cell borders and nuclei were respectively stained with anti E-cadherin and DAPI. Bar = 20 μm. Upper panel, representative images of one optical section taken at the level of the apical junctional complex; lower panel, quantitative analysis done using BlobFinder. Statistical analysis done with One-Way ANOVA followed by Bonferroni's post test. **p<0.01. C) Transfection of a dominant active form of GEF-H1 (GEF-H1 C53R) into parental cells induces the formation of abundant actin stress fibers, while the transfection of a dominant negative GEF-H1 (GEF-H1 Y393A) into ZO-2 KD cells decreases the amount of stress fibers. Cells were transfected with both EGFP and GEF-H1 C53R or GEF-H1 Y393A in order to identify in green the transfected cells by the expression of EGFP. *, transfected cell. D) A higher amount of phosphorylated GEF-H1 at Ser886 is detected in parental than in ZO-2 KD cells. Western blot done with lysates derived from parental and ZO-2 KD cells using specific antibodies against p-GEF-H1 Ser886. Actin was used as loading control. Left panel, representative image; right panel, quantitative analysis. Results from 4 independent experiments. Statistical analysis done with Student's t-test. *p=0.02. E) Cell border staining by GEF-H1 is more pronounced in ZO-2 KD than in parental cells. In parental cells, GEF-H1 stains the cell borders and Golgi (arrow). In ZO-2 KD cells, GEF-H1 staining at Golgi is lost. Immunofluorescence done with specific antibodies against GEF-H1 and ZO-2. Nuclei were stained with DAPI. Bar = 40 μm. F) The amount of GEF-H1 present in the plasma membrane fraction is higher in ZO-2 KD cells than in parental MDCK cells. The plasma membrane fractionation assay was analyzed by Western blot employing antibodies against GEF-H1 and the β1 subunit of the Na^+, K^+-ATPase. The latter is a specific plasma membrane marker. Left, representative blot

image; right densitometric analysis. Statistical analysis done with Student's t-test with Welch's correction; $p<0.05$.

Figure 8. In ZO-2 KD cells cingulin is more abundant but less phosphorylated, and does not associate to microtubules at the TJ and instead recruits GEF-H1. A) Immunofluorescence done in parental and ZO-2 KD cells, with specific antibodies against ZO-2, paracingulin and cingulin. Bar = 40 μm. B) Western blots and corresponding densitometric analysis. Student's *t* test, paracingulin **p=0.0072; cingulin **p=0.0091; results from at least 3 independent experiments. C) PLA assay done in parental and ZO-2 KD MDCK cells with a rabbit polyclonal antibody against cingulin and a mouse monoclonal antibody against GEF-H1. Upper panels, representative images; arrow, positive PLA spots at the cell borders; lower panel, quantitative analysis done using BlobFinder. Statistical analysis done with One-Way ANOVA followed by Bonferroni's post test, **p<0.01; ***p<0.001. Bar = 20 μm. D) The lack of ZO-2 compromises the appearance of microtubules at the cell borders, while treatment with 50 μM forskolin for 24 h or hZO-2 transfection restores the appearance of microtubules. Immunofluorescence done with an antibody against β-tubulin. ZO-2 KD cells transfected with hZO-2 were identified with an antibody against ZO-2 (blue). Arrows indicates β-tubulin staining at the cell borders. Bar = 40 μm. E) The phosphorylation of cingulin diminishes in ZO-2 KD cells, evidenced by faster electrophoretic mobility that is restored after treatment with 50 μM forskolin for 24 h, or hZO-2 transfection. The mobility shift detection assay for cingulin was done running the extracts of parental and ZO-2 KD cells on a Phos-tag SDS-PAGE. F) The interaction of cingulin with β-tubulin diminishes in ZO-2 KD cells and is up-regulated after treatment with 50 μM forskolin for 24 h, or hZO-2 transfection. Cingulin was immunoprecipitated with a specific antibody, from parental and ZO-2 KD cells extracts. The immunoprecipitate was then run on a SDS-PAGE and blotted with antibodies against cingulin and β-tubulin.

Figure 9. ZO-2 KD cells exhibit a lower peak of TER and instead develop a higher TER at steady state that is accompanied by a reduced permeability and a decreased expression of claudin-2 and an increase of claudin-4. A) During the Ca-switch, ZO-2 KD cells display a lower peak of TER than parental cells, which can be restored by ZO-2 transfection. At steady state (inset), ZO-2 KD cells have a higher TER than parental cells. TER was continuously measured during the Ca-switch, using the CellZscope system. The graph presents the mean ± SD of data from six monolayers plated on Transwells. Statistical analysis done with One-Way ANOVA followed by Bonferroni's post test ***, $p<0.001$. B) At steady state (40 h after the Ca-switch), ZO-2 KD cells display a lower paracellular passage of 10 kDa FITC-Dextran (FD10) and 70 kDa FITC-Dextran (FD70), measured in the apical to basolateral direction, than parental cells. Transfection of hZO-2 into ZO-2 KD monolayers restores the paracellular flux of FD10 to that of parental cells and elevates the transit of FD70. Data from three independent monolayers. Statistical analysis determined using the One-Way ANOVA followed by Bonferroni post test. *, $p< 0.05$; ***, $p<0.001$. C) Immunofluorescence detection of claudins -2 and -4 in MDCK parental and ZO-2 KD

cells before the Ca-switch (0 h), at the TER peak and at steady state. Bar = 20 μm. D) In MDCK ZO-2 KD cells, the Western blot shows a decreased expression of claudin-2 and an increased amount of claudin-4, in comparison to parental cells. Upper panels, representative images; lower panels, statistical analysis of 4 independent experiments, done with a Student's *t* test.***p=0.0002; **p=0.002. E) In MDCK ZO-2 KD cells, the Western blot shows a similar expression of GATA-4 in comparison to parental cells. Results obtained from at least three independent experiments. Left, representative image; right, densitometric analysis. Statistical analysis done with One way Annova followed by Bonferroni's post test **p<0.01, ***p<0.001. F) By qRT-PCR we detected no differences in mRNA for claudin-2 between parental and ZO-2 KD cells, but found an increase in the mRNA for claudin-4 in ZO-2 KD cells. Acidic ribosomal phosphoprotein P0 (PRP0) amplified as loading control.

Figure 10. The absence of ZO-2 activates Cdc42, produces a misorientation of the mitotic spindle and in 3D cultures triggers the formation of cysts with multiple lumens. A) Representative *y* sections showing the mitotic spindle orientation in parental and ZO-2 KD MDCK cells. Cells were plated at subconfluent density and 24 h later the monolayers were fixed and processed for immunofluorescence with an antibody against β-tubulin (green) for the detection of the mitotic spindle. Actin was observed with rhodaminated phalloidin (red) and nuclei were stained with DAPI. Bar = 20 μm. B) Radial histograms showing the percentage of cells in metaphase with different angles of mitotic spindle. The percentage of cells with mitotic spindles parallel to the substrate surface (0-10º angle), decreases from 56% in parental cultures to 34% in ZO-2 KD cells. Treatment of ZO-2 KD cells with C3, Y27632 or ML-7 decreases this percentage to 17%, 29% and 25% respectively. C) ZO-2 is required for the correct formation of cysts. ZO-2 KD and parental MDCK cells were incubated with Matrigel and the cyst developed, were observed 10 days later. Cysts were fixed and processed for immunofluorescence with antibodies against E-cadherin (green) and gp135/podocalyxin (red). The nuclei were stained with Topro-3 (blue). The images (left panel) and the graph with the quantitated data (right panel) show that the absence of ZO-2 induces the aberrant formation of multiple lumens per cyst. Statistical analysis done with Student's *t* test **p<0.01. Bar = 20 μm. D) A higher amount of active Cdc42 is present in ZO-2 KD cells in comparison to parental cells. The active form of Cdc42 (Cdc42-GTP) was isolated from parental and ZO-2 KD cells lysates, in a pulldown assay with GST-PAK-CRIB beads. Total cell lysates and pull-downs were resolved on SDS-PAGE gels and analyzed by immunoblotting for Cdc42. Left, representative blot; right, relative fold increase of Cdc42 activation quantitated by densitometric analysis of 4 independent experiments. *p<0.04.

Figure 11. **The lack of ZO-2 changes cell architecture and TJ sealing.** Schematic illustration of the changes generated in epithelial cells by the absence of ZO-2.

References

[1] L. Gonzalez-Mariscal, Quiros, M., Diaz-Coranguez M., and Bautista, P., Tight Junctions, in: N. S. (Ed.) Current Frontiers and Perspectives in Cell Biology, InTech, 2012.
[2] L. Gonzalez-Mariscal, A. Betanzos, A. Avila-Flores, MAGUK proteins: structure and role in the tight junction, Seminars in cell & developmental biology, 11 (2000) 315-324.
[3] L. Gonzalez-Mariscal, M. Quiros, M. Diaz-Coranguez, ZO proteins and redox-dependent processes, Antioxidants & redox signaling, 15 (2011) 1235-1253.
[4] M. Itoh, M. Furuse, K. Morita, K. Kubota, M. Saitou, S. Tsukita, Direct binding of three tight junction-associated MAGUKs, ZO-1, ZO-2, and ZO-3, with the COOH termini of claudins, The Journal of cell biology, 147 (1999) 1351-1363.
[5] M. Itoh, K. Morita, S. Tsukita, Characterization of ZO-2 as a MAGUK family member associated with tight as well as adherens junctions with a binding affinity to occludin and alpha catenin, The Journal of biological chemistry, 274 (1999) 5981-5986.
[6] K. Ebnet, C.U. Schulz, M.K. Meyer Zu Brickwedde, G.G. Pendl, D. Vestweber, Junctional adhesion molecule interacts with the PDZ domain-containing proteins AF-6 and ZO-1, The Journal of biological chemistry, 275 (2000) 27979-27988.
[7] A.C. Monteiro, R. Sumagin, C.R. Rankin, G. Leoni, M.J. Mina, D.M. Reiter, T. Stehle, T.S. Dermody, S.A. Schaefer, R.A. Hall, A. Nusrat, C.A. Parkos, JAM-A associates with ZO-2, afadin, and PDZ-GEF1 to activate Rap2c and regulate epithelial barrier function, Molecular biology of the cell, 24 (2013) 2849-2860.
[8] A.S. Fanning, B.J. Jameson, L.A. Jesaitis, J.M. Anderson, The tight junction protein ZO-1 establishes a link between the transmembrane protein occludin and the actin cytoskeleton, The Journal of biological chemistry, 273 (1998) 29745-29753.
[9] P.J. Kausalya, M. Reichert, W. Hunziker, Connexin45 directly binds to ZO-1 and localizes to the tight junction region in epithelial MDCK cells, FEBS letters, 505 (2001) 92-96.
[10] X. Li, C. Olson, S. Lu, N. Kamasawa, T. Yasumura, J.E. Rash, J.I. Nagy, Neuronal connexin36 association with zonula occludens-1 protein (ZO-1) in mouse brain and interaction with the first PDZ domain of ZO-1, The European journal of neuroscience, 19 (2004) 2132-2146.
[11] B.N. Giepmans, W.H. Moolenaar, The gap junction protein connexin43 interacts with the second PDZ domain of the zona occludens-1 protein, Curr Biol, 8 (1998) 931-934.
[12] P.A. Nielsen, A. Baruch, V.I. Shestopalov, B.N. Giepmans, I. Dunia, E.L. Benedetti, N.M. Kumar, Lens connexins alpha3Cx46 and alpha8Cx50 interact with zonula occludens protein-1 (ZO-1), Molecular biology of the cell, 14 (2003) 2470-2481.
[13] M. Itoh, A. Nagafuchi, S. Moroi, S. Tsukita, Involvement of ZO-1 in cadherin-based cell adhesion through its direct binding to alpha catenin and actin filaments, The Journal of cell biology, 138 (1997) 181-192.
[14] M.S. Balda, J.M. Anderson, K. Matter, The SH3 domain of the tight junction protein ZO-1 binds to a serine protein kinase that phosphorylates a region C-terminal to this domain, FEBS letters, 399 (1996) 326-332.
[15] A.S. Fanning, T.Y. Ma, J.M. Anderson, Isolation and functional characterization of the actin binding region in the tight junction protein ZO-1, FASEB journal : official

publication of the Federation of American Societies for Experimental Biology, 16 (2002) 1835-1837.
[16] E.S. Wittchen, J. Haskins, B.R. Stevenson, Protein interactions at the tight junction. Actin has multiple binding partners, and ZO-1 forms independent complexes with ZO-2 and ZO-3, The Journal of biological chemistry, 274 (1999) 35179-35185.
[17] S.N. Mattagajasingh, S.C. Huang, J.S. Hartenstein, E.J. Benz, Jr., Characterization of the interaction between protein 4.1R and ZO-2. A possible link between the tight junction and the actin cytoskeleton, The Journal of biological chemistry, 275 (2000) 30573-30585.
[18] T. Katsube, M. Takahisa, R. Ueda, N. Hashimoto, M. Kobayashi, S. Togashi, Cortactin associates with the cell-cell junction protein ZO-1 in both Drosophila and mouse, The Journal of biological chemistry, 273 (1998) 29672-29677.
[19] C.M. Van Itallie, J. Holmes, A. Bridges, J.L. Gookin, M.R. Coccaro, W. Proctor, O.R. Colegio, J.M. Anderson, The density of small tight junction pores varies among cell types and is increased by expression of claudin-2, Journal of cell science, 121 (2008) 298-305.
[20] C.J. Watson, M. Rowland, G. Warhurst, Functional modeling of tight junctions in intestinal cell monolayers using polyethylene glycol oligomers, American journal of physiology. Cell physiology, 281 (2001) C388-397.
[21] D. Gunzel, A.S. Yu, Claudins and the modulation of tight junction permeability, Physiological reviews, 93 (2013) 525-569.
[22] A. Nusrat, M. Giry, J.R. Turner, S.P. Colgan, C.A. Parkos, D. Carnes, E. Lemichez, P. Boquet, J.L. Madara, Rho protein regulates tight junctions and perijunctional actin organization in polarized epithelia, Proceedings of the National Academy of Sciences of the United States of America, 92 (1995) 10629-10633.
[23] M. Amano, M. Ito, K. Kimura, Y. Fukata, K. Chihara, T. Nakano, Y. Matsuura, K. Kaibuchi, Phosphorylation and activation of myosin by Rho-associated kinase (Rho-kinase), The Journal of biological chemistry, 271 (1996) 20246-20249.
[24] L. Shen, E.D. Black, E.D. Witkowski, W.I. Lencer, V. Guerriero, E.E. Schneeberger, J.R. Turner, Myosin light chain phosphorylation regulates barrier function by remodeling tight junction structure, Journal of cell science, 119 (2006) 2095-2106.
[25] K. Kimura, M. Ito, M. Amano, K. Chihara, Y. Fukata, M. Nakafuku, B. Yamamori, J. Feng, T. Nakano, K. Okawa, A. Iwamatsu, K. Kaibuchi, Regulation of myosin phosphatase by Rho and Rho-associated kinase (Rho-kinase), Science, 273 (1996) 245-248.
[26] S. Gopalakrishnan, N. Raman, S.J. Atkinson, J.A. Marrs, Rho GTPase signaling regulates tight junction assembly and protects tight junctions during ATP depletion, The American journal of physiology, 275 (1998) C798-809.
[27] T.S. Jou, E.E. Schneeberger, W.J. Nelson, Structural and functional regulation of tight junctions by RhoA and Rac1 small GTPases, The Journal of cell biology, 142 (1998) 101-115.
[28] S. Islas, J. Vega, L. Ponce, L. Gonzalez-Mariscal, Nuclear localization of the tight junction protein ZO-2 in epithelial cells, Experimental cell research, 274 (2002) 138-148.

[29] A. Betanzos, M. Huerta, E. Lopez-Bayghen, E. Azuara, J. Amerena, L. Gonzalez-Mariscal, The tight junction protein ZO-2 associates with Jun, Fos and C/EBP transcription factors in epithelial cells, Experimental cell research, 292 (2004) 51-66.
[30] M. Huerta, R. Munoz, R. Tapia, E. Soto-Reyes, L. Ramirez, F. Recillas-Targa, L. Gonzalez-Mariscal, E. Lopez-Bayghen, Cyclin D1 is transcriptionally down-regulated by ZO-2 via an E box and the transcription factor c-Myc, Molecular biology of the cell, 18 (2007) 4826-4836.
[31] E. Lopez-Bayghen, Jaramillo B. E., Huerta, M., Betanzos, A., and Gonzalez-Marical, L., TJ proteins that make round trips to the nucleus, in: L. Gonzalez-Mariscal (Ed.) Tight Junctions, Landes Bioscience and Springer Science+Business Media, Place Published, 2006, pp. 76-100.
[32] D. Chamorro, L. Alarcon, A. Ponce, R. Tapia, H. Gonzalez-Aguilar, M. Robles-Flores, T. Mejia-Castillo, J. Segovia, Y. Bandala, E. Juaristi, L. Gonzalez-Mariscal, Phosphorylation of zona occludens-2 by protein kinase C epsilon regulates its nuclear exportation, Molecular biology of the cell, 20 (2009) 4120-4129.
[33] M. Quiros, L. Alarcon, A. Ponce, T. Giannakouros, L. Gonzalez-Mariscal, The intracellular fate of zonula occludens 2 is regulated by the phosphorylation of SR repeats and the phosphorylation/O-GlcNAcylation of S257, Mol Biol Cell, 24 (2013) 2528-2543.
[34] K. Umeda, J. Ikenouchi, S. Katahira-Tayama, K. Furuse, H. Sasaki, M. Nakayama, T. Matsui, S. Tsukita, M. Furuse, S. Tsukita, ZO-1 and ZO-2 independently determine where claudins are polymerized in tight-junction strand formation, Cell, 126 (2006) 741-754.
[35] V.E. Carlton, B.Z. Harris, E.G. Puffenberger, A.K. Batta, A.S. Knisely, D.L. Robinson, K.A. Strauss, B.L. Shneider, W.A. Lim, G. Salen, D.H. Morton, L.N. Bull, Complex inheritance of familial hypercholanemia with associated mutations in TJP2 and BAAT, Nature genetics, 34 (2003) 91-96.
[36] J. Xu, F. Anuar, S.M. Ali, M.Y. Ng, D.C. Phua, W. Hunziker, Zona occludens-2 is critical for blood-testis barrier integrity and male fertility, Molecular biology of the cell, 20 (2009) 4268-4277.
[37] C.M. Van Itallie, A.S. Fanning, A. Bridges, J.M. Anderson, ZO-1 stabilizes the tight junction solute barrier through coupling to the perijunctional cytoskeleton, Mol Biol Cell, 20 (2009) 3930-3940.
[38] S. Hernandez, B. Chavez Munguia, L. Gonzalez-Mariscal, ZO-2 silencing in epithelial cells perturbs the gate and fence function of tight junctions and leads to an atypical monolayer architecture, Experimental cell research, 313 (2007) 1533-1547.
[39] A. Dominguez-Calderon, A. Avila-Flores, A. Ponce, E. Lopez-Bayghen, J.V. Calderon-Salinas, J. Luis Reyes, B. Chavez-Munguia, J. Segovia, C. Angulo, L. Ramirez, H. Gallego-Gutierrez, L. Alarcon, D. Martin-Tapia, P. Bautista-Garcia, L. Gonzalez-Mariscal, ZO-2 silencing induces renal hypertrophy through a cell cycle mechanism and the activation of YAP and the mTOR pathway, Molecular biology of the cell, 27 (2016) 1581-1595.
[40] J. Carretero-Ortega, C.T. Walsh, R. Hernandez-Garcia, G. Reyes-Cruz, J.H. Brown, J. Vazquez-Prado, Phosphatidylinositol 3,4,5-triphosphate-dependent Rac exchanger 1 (P-Rex-1), a guanine nucleotide exchange factor for Rac, mediates angiogenic responses to stromal cell-derived factor-1/chemokine stromal cell derived factor-1

(SDF-1/CXCL-12) linked to Rac activation, endothelial cell migration, and in vitro angiogenesis, Mol Pharmacol, 77 (2010) 435-442.
[41] O. Pertz, L. Hodgson, R.L. Klemke, K.M. Hahn, Spatiotemporal dynamics of RhoA activity in migrating cells, Nature, 440 (2006) 1069-1072.
[42] E. Kardash, J. Bandemer, E. Raz, Imaging protein activity in live embryos using fluorescence resonance energy transfer biosensors, Nat Protoc, 6 (2011) 1835-1846.
[43] A. Allalou, C. Wahlby, BlobFinder, a tool for fluorescence microscopy image cytometry, Comput Methods Programs Biomed, 94 (2009) 58-65.
[44] P. Nava, S. Lopez, C.F. Arias, S. Islas, L. Gonzalez-Mariscal, The rotavirus surface protein VP8 modulates the gate and fence function of tight junctions in epithelial cells, J Cell Sci, 117 (2004) 5509-5519.
[45] Z. Lu, H. Kim do, J. Fan, Q. Lu, K. Verbanac, L. Ding, R. Renegar, Y.H. Chen, A non-tight junction function of claudin-7-Interaction with integrin signaling in suppressing lung cancer cell proliferation and detachment, Molecular cancer, 14 (2015) 120.
[46] L. Ding, Z. Lu, O. Foreman, R. Tatum, Q. Lu, R. Renegar, J. Cao, Y.H. Chen, Inflammation and disruption of the mucosal architecture in claudin-7-deficient mice, Gastroenterology, 142 (2012) 305-315.
[47] I. Rabinovitz, A.M. Mercurio, The integrin alpha6beta4 functions in carcinoma cell migration on laminin-1 by mediating the formation and stabilization of actin-containing motility structures, J Cell Biol, 139 (1997) 1873-1884.
[48] T.Y. Huang, C. DerMardirossian, G.M. Bokoch, Cofilin phosphatases and regulation of actin dynamics, Curr Opin Cell Biol, 18 (2006) 26-31.
[49] D. Pandey, P. Goyal, S. Dwivedi, W. Siess, Unraveling a novel Rac1-mediated signaling pathway that regulates cofilin dephosphorylation and secretion in thrombin-stimulated platelets, Blood, 114 (2009) 415-424.
[50] R. Pankov, Y. Endo, S. Even-Ram, M. Araki, K. Clark, E. Cukierman, K. Matsumoto, K.M. Yamada, A Rac switch regulates random versus directionally persistent cell migration, J Cell Biol, 170 (2005) 793-802.
[51] I. Dang, R. Gorelik, C. Sousa-Blin, E. Derivery, C. Guerin, J. Linkner, M. Nemethova, J.G. Dumortier, F.A. Giger, T.A. Chipysheva, V.D. Ermilova, S. Vacher, V. Campanacci, I. Herrada, A.G. Planson, S. Fetics, V. Henriot, V. David, K. Oguievetskaia, G. Lakisic, F. Pierre, A. Steffen, A. Boyreau, N. Peyrieras, K. Rottner, S. Zinn-Justin, J. Cherfils, I. Bieche, A.Y. Alexandrova, N.B. David, J.V. Small, J. Faix, L. Blanchoin, A. Gautreau, Inhibitory signalling to the Arp2/3 complex steers cell migration, Nature, 503 (2013) 281-284.
[52] M. Bruewer, A.M. Hopkins, M.E. Hobert, A. Nusrat, J.L. Madara, RhoA, Rac1, and Cdc42 exert distinct effects on epithelial barrier via selective structural and biochemical modulation of junctional proteins and F-actin, Am J Physiol Cell Physiol, 287 (2004) C327-335.
[53] S.J. Terry, C. Zihni, A. Elbediwy, E. Vitiello, I.V. Leefa Chong San, M.S. Balda, K. Matter, Spatially restricted activation of RhoA signalling at epithelial junctions by p114RhoGEF drives junction formation and morphogenesis, Nat Cell Biol, 13 (2011) 159-166.
[54] F. Matsumura, Regulation of myosin II during cytokinesis in higher eukaryotes, Trends in cell biology, 15 (2005) 371-377.

[55] S. Nandadasa, Q. Tao, N.R. Menon, J. Heasman, C. Wylie, N- and E-cadherins in Xenopus are specifically required in the neural and non-neural ectoderm, respectively, for F-actin assembly and morphogenetic movements, Development, 136 (2009) 1327-1338.
[56] K. Aktories, I. Just, In vitro ADP-ribosylation of Rho by bacterial ADP-ribosyltransferases, Methods Enzymol, 256 (1995) 184-195.
[57] S. Narumiya, T. Ishizaki, M. Uehata, Use and properties of ROCK-specific inhibitor Y-27632, Methods Enzymol, 325 (2000) 273-284.
[58] M. Saitoh, T. Ishikawa, S. Matsushima, M. Naka, H. Hidaka, Selective inhibition of catalytic activity of smooth muscle myosin light chain kinase, J Biol Chem, 262 (1987) 7796-7801.
[59] S. Aijaz, F. D'Atri, S. Citi, M.S. Balda, K. Matter, Binding of GEF-H1 to the tight junction-associated adaptor cingulin results in inhibition of Rho signaling and G1/S phase transition, Dev Cell, 8 (2005) 777-786.
[60] L. Guillemot, S. Paschoud, L. Jond, A. Foglia, S. Citi, Paracingulin regulates the activity of Rac1 and RhoA GTPases by recruiting Tiam1 and GEF-H1 to epithelial junctions, Mol Biol Cell, 19 (2008) 4442-4453.
[61] M.G. Callow, S. Zozulya, M.L. Gishizky, B. Jallal, T. Smeal, PAK4 mediates morphological changes through the regulation of GEF-H1, Journal of cell science, 118 (2005) 1861-1872.
[62] G. Benais-Pont, A. Punn, C. Flores-Maldonado, J. Eckert, G. Raposo, T.P. Fleming, M. Cereijido, M.S. Balda, K. Matter, Identification of a tight junction-associated guanine nucleotide exchange factor that activates Rho and regulates paracellular permeability, The Journal of cell biology, 160 (2003) 729-740.
[63] T. Yano, T. Matsui, A. Tamura, M. Uji, S. Tsukita, The association of microtubules with tight junctions is promoted by cingulin phosphorylation by AMPK, The Journal of cell biology, 203 (2013) 605-614.
[64] M. Egawa, H. Kamata, A. Kushiyama, H. Sakoda, M. Fujishiro, N. Horike, M. Yoneda, Y. Nakatsu, G. Ying, Z. Jun, Y. Tsuchiya, K. Takata, H. Kurihara, T. Asano, Long-term forskolin stimulation induces AMPK activation and thereby enhances tight junction formation in human placental trophoblast BeWo cells, Placenta, 29 (2008) 1003-1008.
[65] S. Amasheh, N. Meiri, A.H. Gitter, T. Schoneberg, J. Mankertz, J.D. Schulzke, M. Fromm, Claudin-2 expression induces cation-selective channels in tight junctions of epithelial cells, Journal of cell science, 115 (2002) 4969-4976.
[66] A.S. Yu, M.H. Cheng, S. Angelow, D. Gunzel, S.A. Kanzawa, E.E. Schneeberger, M. Fromm, R.D. Coalson, Molecular basis for cation selectivity in claudin-2-based paracellular pores: identification of an electrostatic interaction site, The Journal of general physiology, 133 (2009) 111-127.
[67] C.M. Van Itallie, A.S. Fanning, J.M. Anderson, Reversal of charge selectivity in cation or anion-selective epithelial lines by expression of different claudins, American journal of physiology. Renal physiology, 285 (2003) F1078-1084.
[68] M. Furuse, K. Furuse, H. Sasaki, S. Tsukita, Conversion of zonulae occludentes from tight to leaky strand type by introducing claudin-2 into Madin-Darby canine kidney I cells, The Journal of cell biology, 153 (2001) 263-272.

[69] C. Van Itallie, C. Rahner, J.M. Anderson, Regulated expression of claudin-4 decreases paracellular conductance through a selective decrease in sodium permeability, The Journal of clinical investigation, 107 (2001) 1319-1327.
[70] J. Hou, A. Renigunta, J. Yang, S. Waldegger, Claudin-4 forms paracellular chloride channel in the kidney and requires claudin-8 for tight junction localization, Proceedings of the National Academy of Sciences of the United States of America, 107 (2010) 18010-18015.
[71] L. Guillemot, D. Spadaro, S. Citi, The junctional proteins cingulin and paracingulin modulate the expression of tight junction protein genes through GATA-4, PloS one, 8 (2013) e55873.
[72] S. Etienne-Manneville, A. Hall, Integrin-mediated activation of Cdc42 controls cell polarity in migrating astrocytes through PKCzeta, Cell, 106 (2001) 489-498.
[73] A.B. Jaffe, N. Kaji, J. Durgan, A. Hall, Cdc42 controls spindle orientation to position the apical surface during epithelial morphogenesis, The Journal of cell biology, 183 (2008) 625-633.
[74] O. Tornavaca, M. Chia, N. Dufton, L.O. Almagro, D.E. Conway, A.M. Randi, M.A. Schwartz, K. Matter, M.S. Balda, ZO-1 controls endothelial adherens junctions, cell-cell tension, angiogenesis, and barrier formation, The Journal of cell biology, 208 (2015) 821-838.
[75] A.S. Fanning, C.M. Van Itallie, J.M. Anderson, Zonula occludens-1 and -2 regulate apical cell structure and the zonula adherens cytoskeleton in polarized epithelia, Molecular biology of the cell, 23 (2012) 577-590.
[76] Y. Yamazaki, K. Umeda, M. Wada, S. Nada, M. Okada, S. Tsukita, S. Tsukita, ZO-1- and ZO-2-dependent integration of myosin-2 to epithelial zonula adherens, Molecular biology of the cell, 19 (2008) 3801-3811.
[77] D.W. Dumbauld, H. Shin, N.D. Gallant, K.E. Michael, H. Radhakrishna, A.J. Garcia, Contractility modulates cell adhesion strengthening through focal adhesion kinase and assembly of vinculin-containing focal adhesions, Journal of cellular physiology, 223 (2010) 746-756.
[78] A.J. Ridley, H.F. Paterson, C.L. Johnston, D. Diekmann, A. Hall, The small GTP-binding protein rac regulates growth factor-induced membrane ruffling, Cell, 70 (1992) 401-410.
[79] K. Tumaneng, K. Schlegelmilch, R.C. Russell, D. Yimlamai, H. Basnet, N. Mahadevan, J. Fitamant, N. Bardeesy, F.D. Camargo, K.L. Guan, YAP mediates crosstalk between the Hippo and PI(3)K-TOR pathways by suppressing PTEN via miR-29, Nature cell biology, 14 (2012) 1322-1329.
[80] Z. Lin, P. Zhou, A. von Gise, F. Gu, Q. Ma, J. Chen, H. Guo, P.R. van Gorp, D.Z. Wang, W.T. Pu, Pi3kcb links Hippo-YAP and PI3K-AKT signaling pathways to promote cardiomyocyte proliferation and survival, Circulation research, 116 (2015) 35-45.
[81] M. Nishita, Y. Wang, C. Tomizawa, A. Suzuki, R. Niwa, T. Uemura, K. Mizuno, Phosphoinositide 3-kinase-mediated activation of cofilin phosphatase Slingshot and its role for insulin-induced membrane protrusion, J Biol Chem, 279 (2004) 7193-7198.
[82] E. Luczka, L. Syne, B. Nawrocki-Raby, C. Kileztky, W. Hunziker, P. Birembaut, C. Gilles, M. Polette, Regulation of membrane-type 1 matrix metalloproteinase expression by zonula occludens-2 in human lung cancer cells, Clinical & experimental metastasis, (2013).

[83] A.M. Hopkins, S.V. Walsh, P. Verkade, P. Boquet, A. Nusrat, Constitutive activation of Rho proteins by CNF-1 influences tight junction structure and epithelial barrier function, Journal of cell science, 116 (2003) 725-742.
[84] T.S. Jou, W.J. Nelson, Effects of regulated expression of mutant RhoA and Rac1 small GTPases on the development of epithelial (MDCK) cell polarity, The Journal of cell biology, 142 (1998) 85-100.
[85] S.N. Samarin, A.I. Ivanov, G. Flatau, C.A. Parkos, A. Nusrat, Rho/Rho-associated kinase-II signaling mediates disassembly of epithelial apical junctions, Molecular biology of the cell, 18 (2007) 3429-3439.
[86] K. Katoh, Y. Kano, M. Amano, H. Onishi, K. Kaibuchi, K. Fujiwara, Rho-kinase--mediated contraction of isolated stress fibers, The Journal of cell biology, 153 (2001) 569-584.
[87] M. Cereijido, L. Gonzalez-Mariscal, L. Borboa, Occluding junctions and paracellular pathways studied in monolayers of MDCK cells, The Journal of experimental biology, 106 (1983) 205-215.
[88] L. Gonzalez-Mariscal, B. Chavez de Ramirez, M. Cereijido, Tight junction formation in cultured epithelial cells (MDCK), The Journal of membrane biology, 86 (1985) 113-125.
[89] M.A. Odenwald, W. Choi, A. Buckley, N. Shashikanth, N.E. Joseph, Y. Wang, M.H. Warren, M.M. Buschmann, R. Pavlyuk, J. Hildebrand, B. Margolis, A.S. Fanning, J.R. Turner, ZO-1 interactions with F-actin and occludin direct epithelial polarization and single lumen specification in 3D culture, Journal of cell science, 130 (2017) 243-259.
[90] L. Gonzalez-Mariscal, A. Avila, A. Betanzos, Tight Junctions, 2nd ed., CRC Press, Place Published, 2001.
[91] B.E. Tanos, A.E. Perez Bay, S. Salvarezza, I. Vivanco, I. Mellinghoff, M. Osman, D.B. Sacks, E. Rodriguez-Boulan, IQGAP1 controls tight junction formation through differential regulation of claudin recruitment, Journal of cell science, 128 (2015) 853-862.
[92] L. Guillemot, S. Citi, Cingulin regulates claudin-2 expression and cell proliferation through the small GTPase RhoA, Molecular biology of the cell, 17 (2006) 3569-3577.
[93] L. Guillemot, E. Hammar, C. Kaister, J. Ritz, D. Caille, L. Jond, C. Bauer, P. Meda, S. Citi, Disruption of the cingulin gene does not prevent tight junction formation but alters gene expression, Journal of cell science, 117 (2004) 5245-5256.
[94] J.M. Vasiliev, T. Omelchenko, I.M. Gelfand, H.H. Feder, E.M. Bonder, Rho overexpression leads to mitosis-associated detachment of cells from epithelial sheets: a link to the mechanism of cancer dissemination, Proceedings of the National Academy of Sciences of the United States of America, 101 (2004) 12526-12530.
[95] S. Etienne-Manneville, A. Hall, Cdc42 regulates GSK-3beta and adenomatous polyposis coli to control cell polarity, Nature, 421 (2003) 753-756.
[96] L. Gonzalez-Mariscal, J. Miranda, J.M. Ortega-Olvera, H. Gallego-Gutierrez, A. Raya-Sandino, O. Vargas-Sierra, Zonula Occludens Proteins in Cancer, Current Pathobiology Reports, 4 (2016) 107-116.

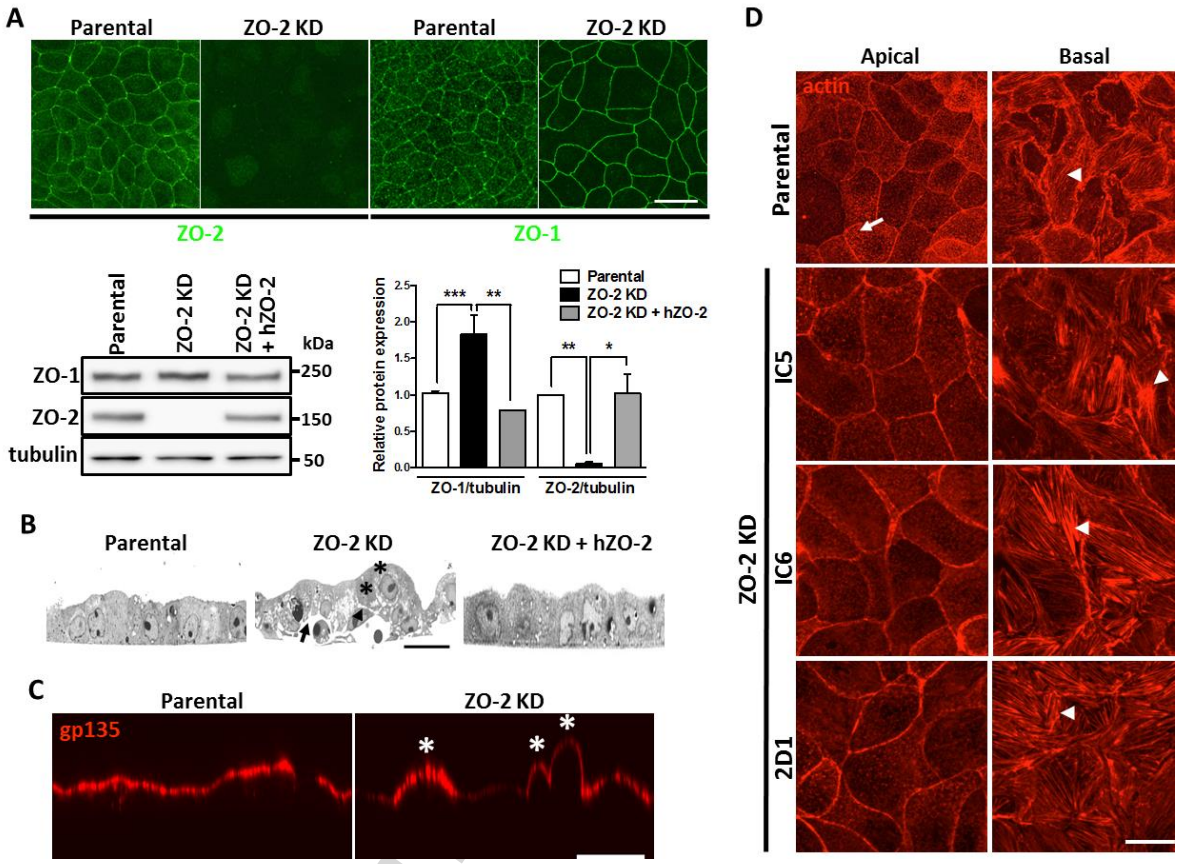

Figure 1

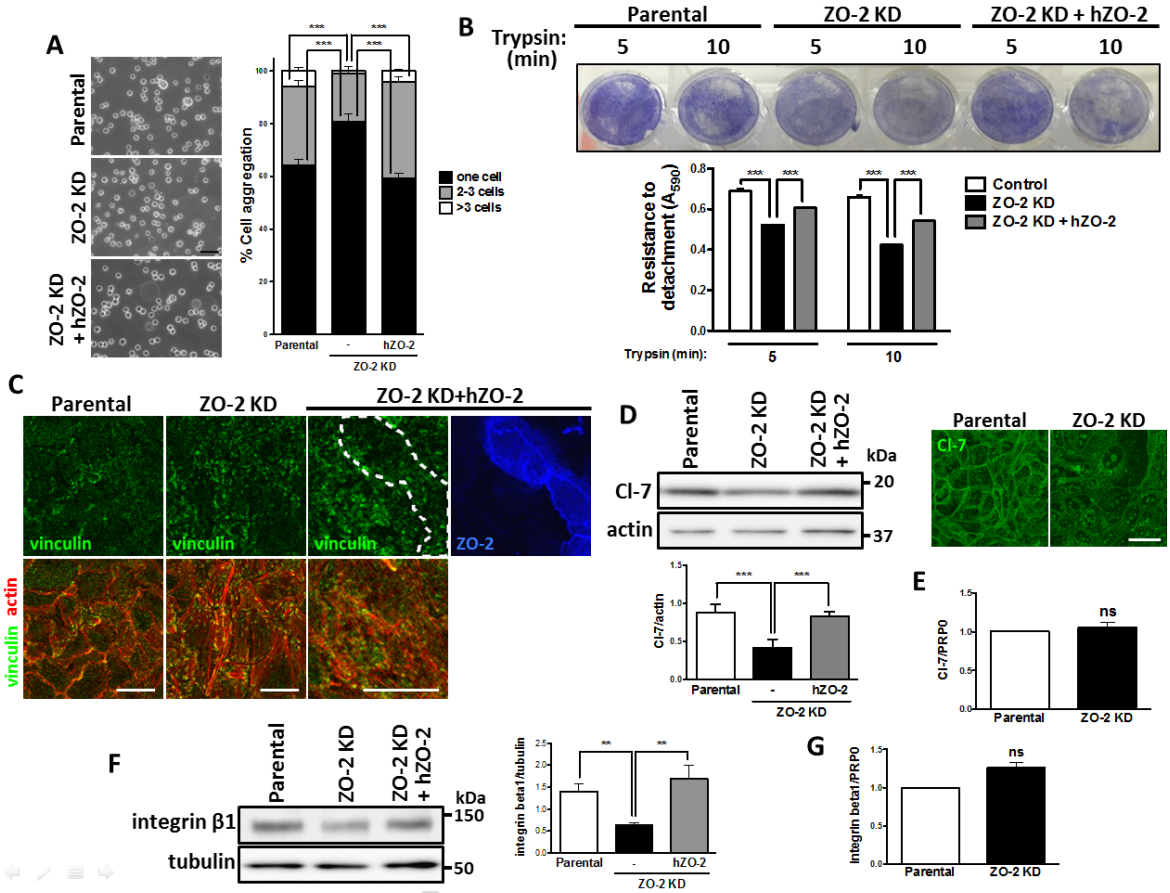

Figure 2

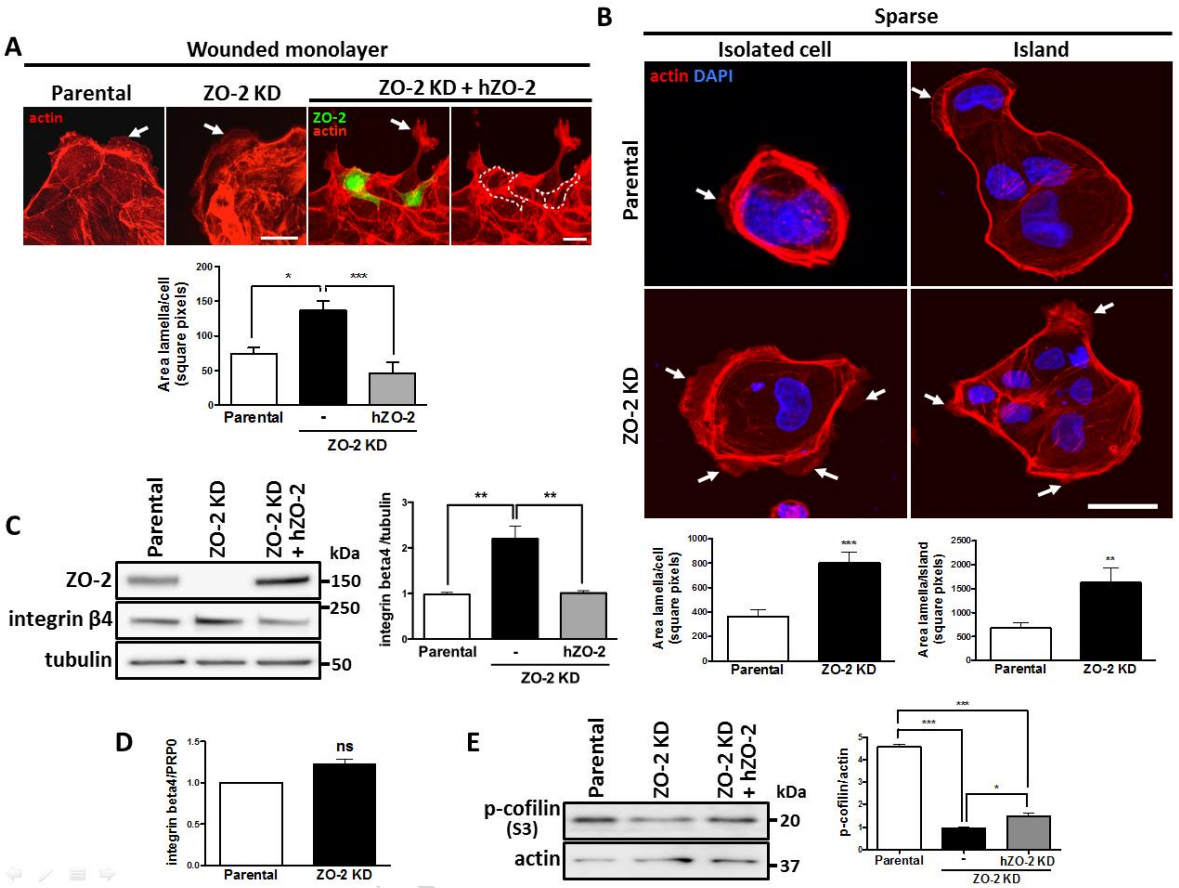

Figure 3

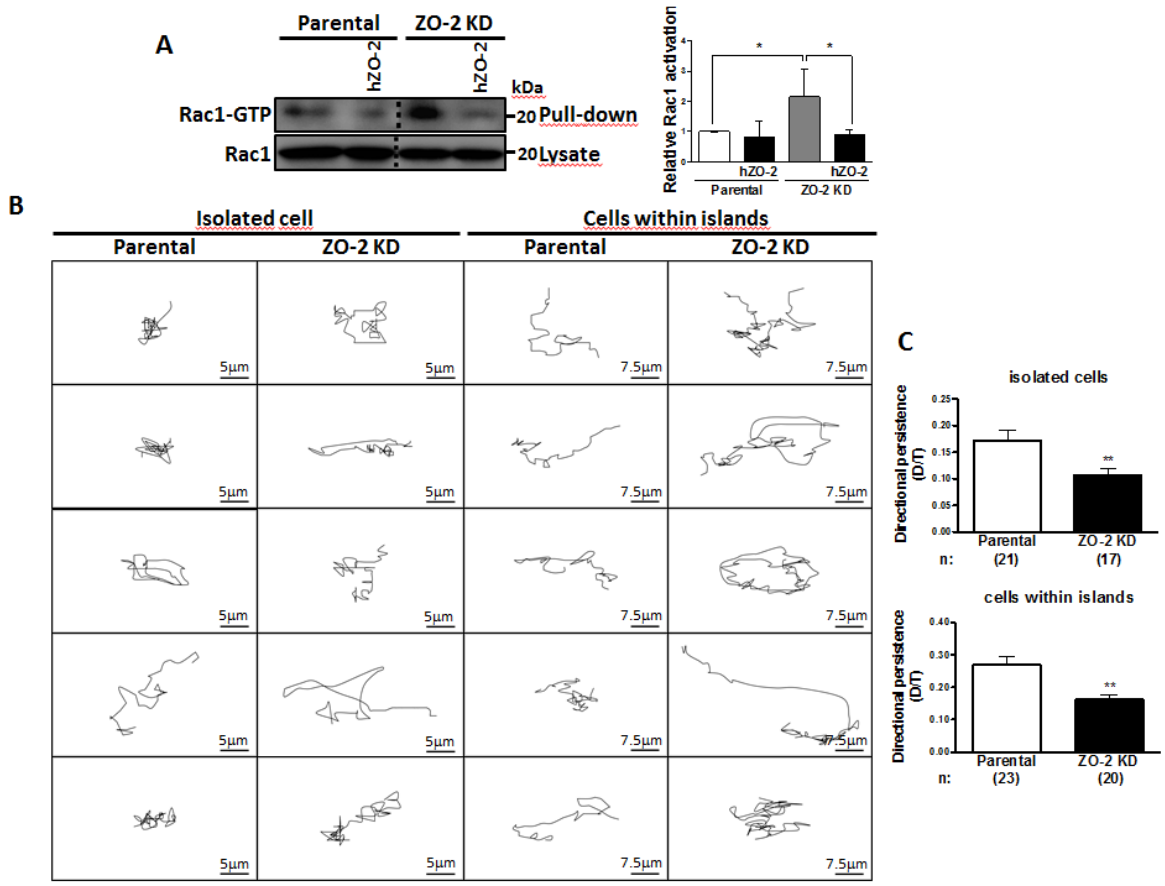

Figure 4.1

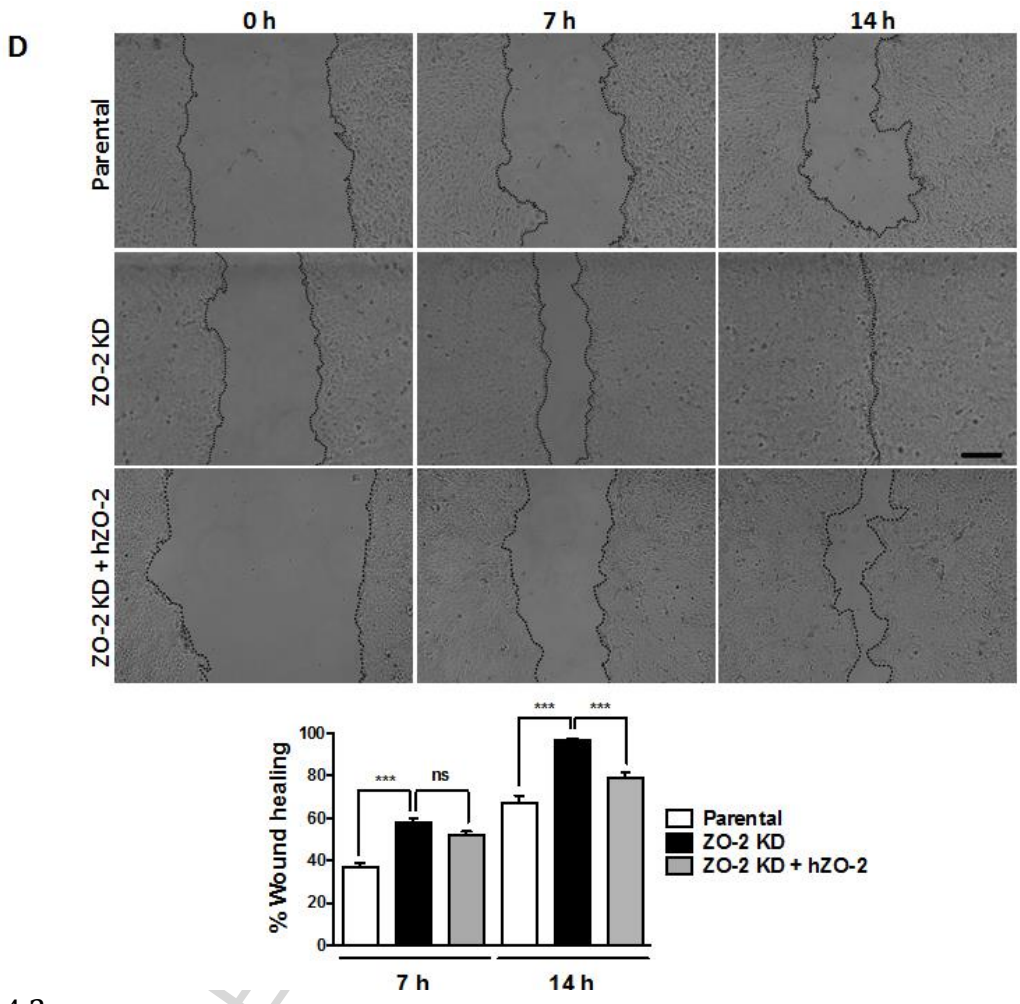

Figure 4.2

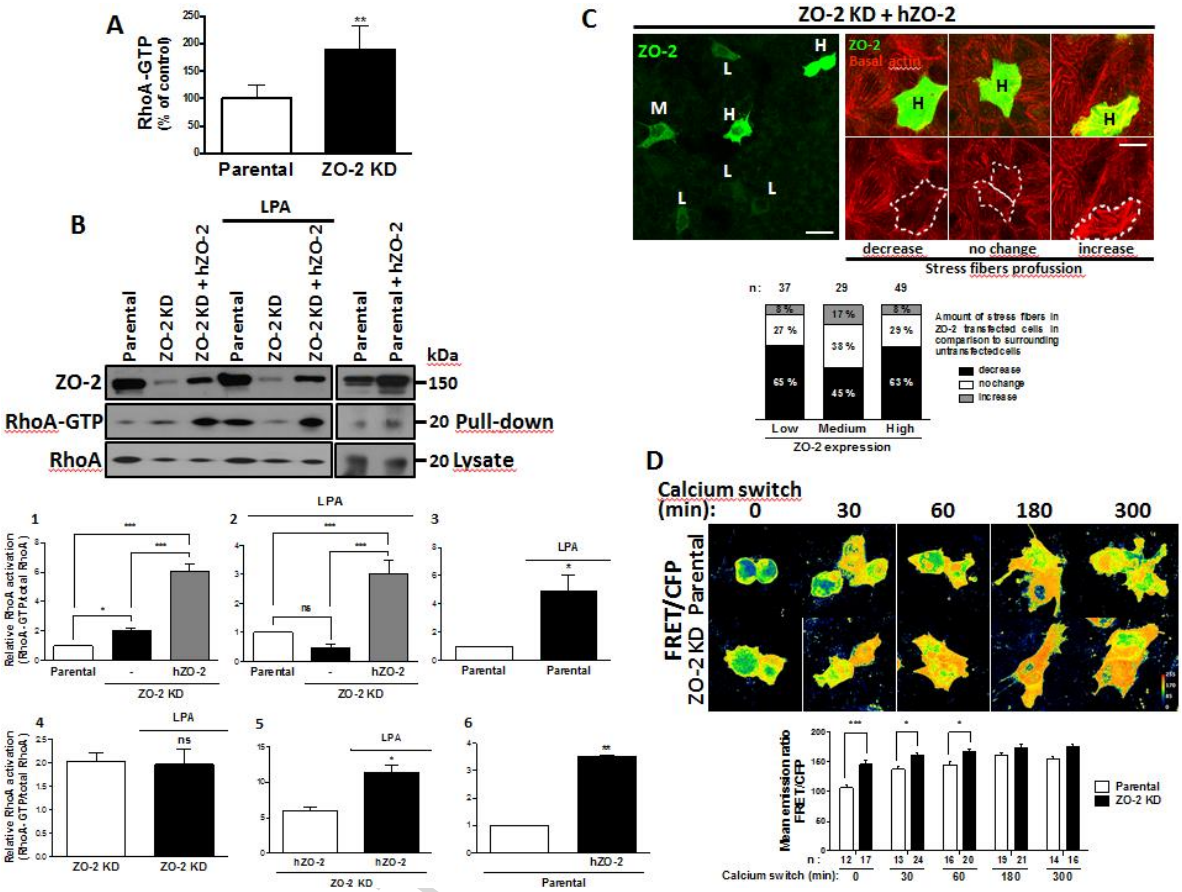

Figure 5

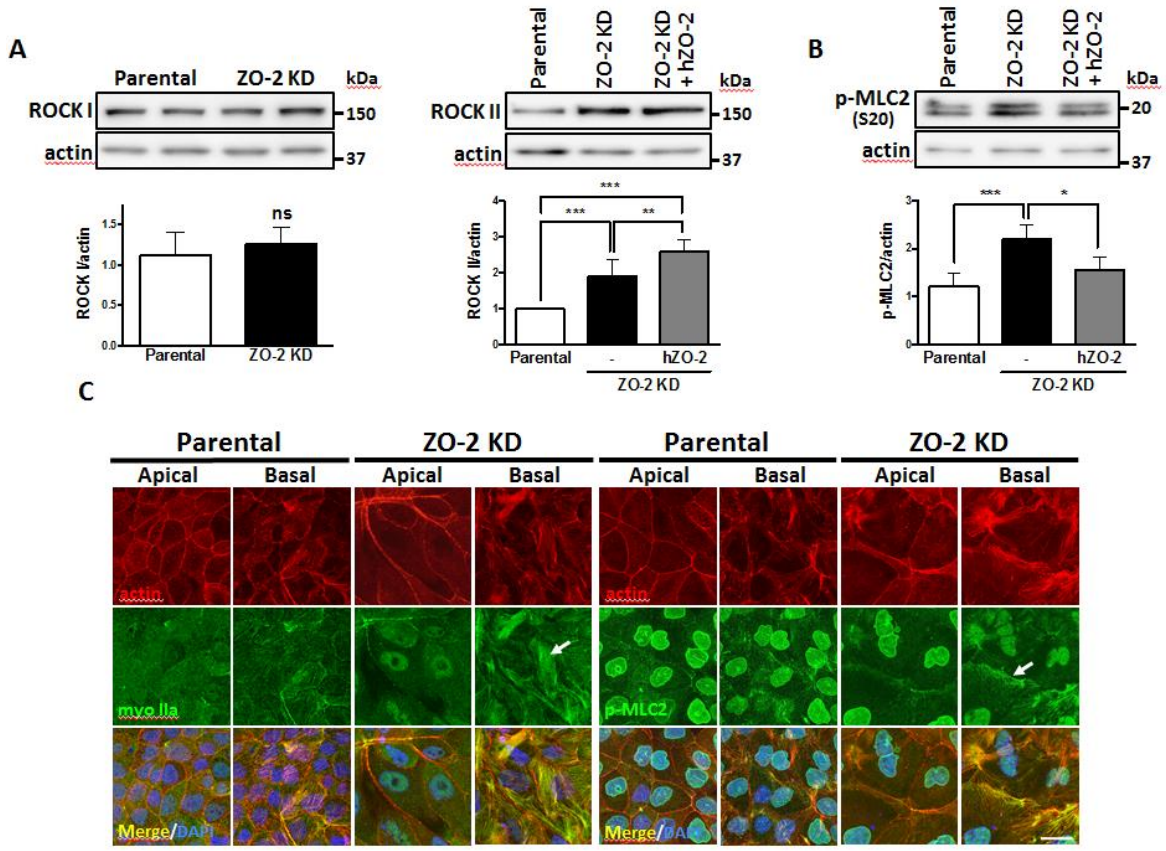

Figure 6.1

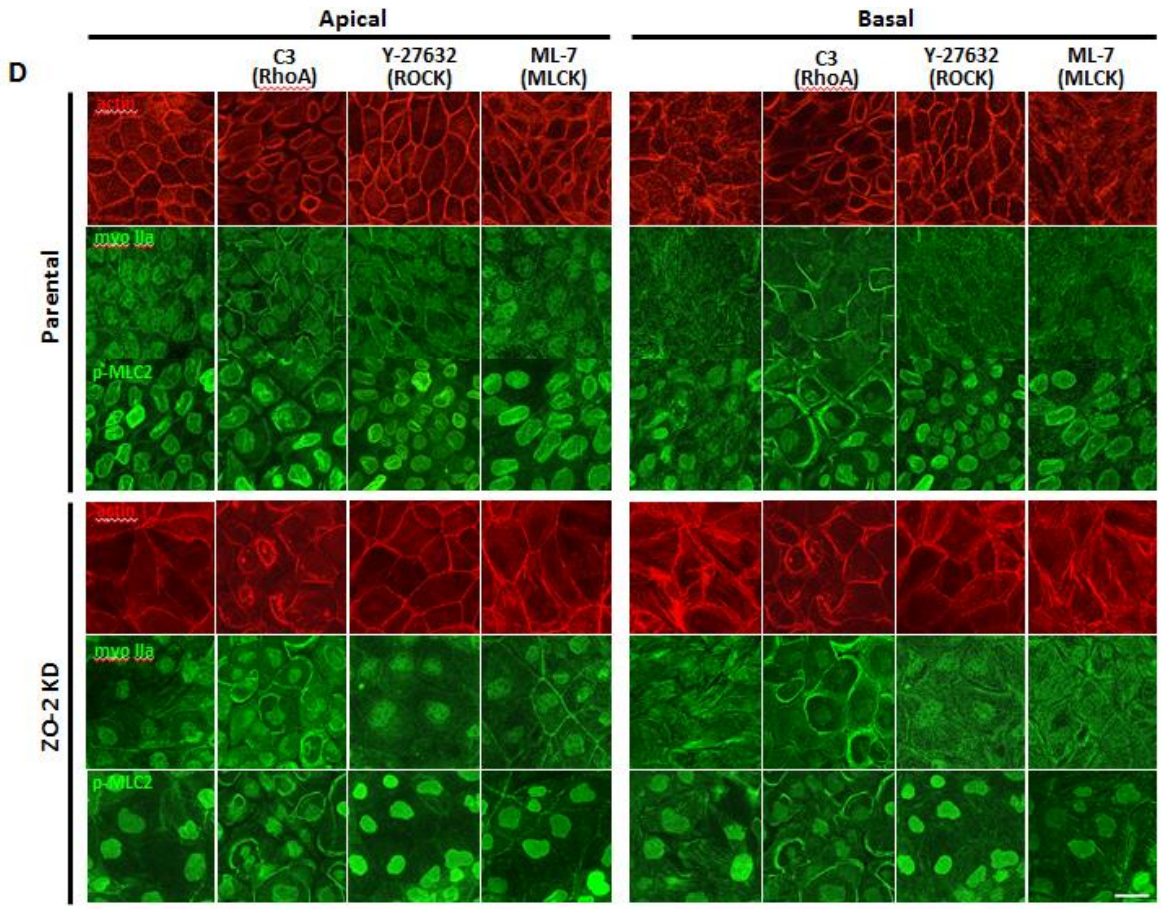

Figure 6.2

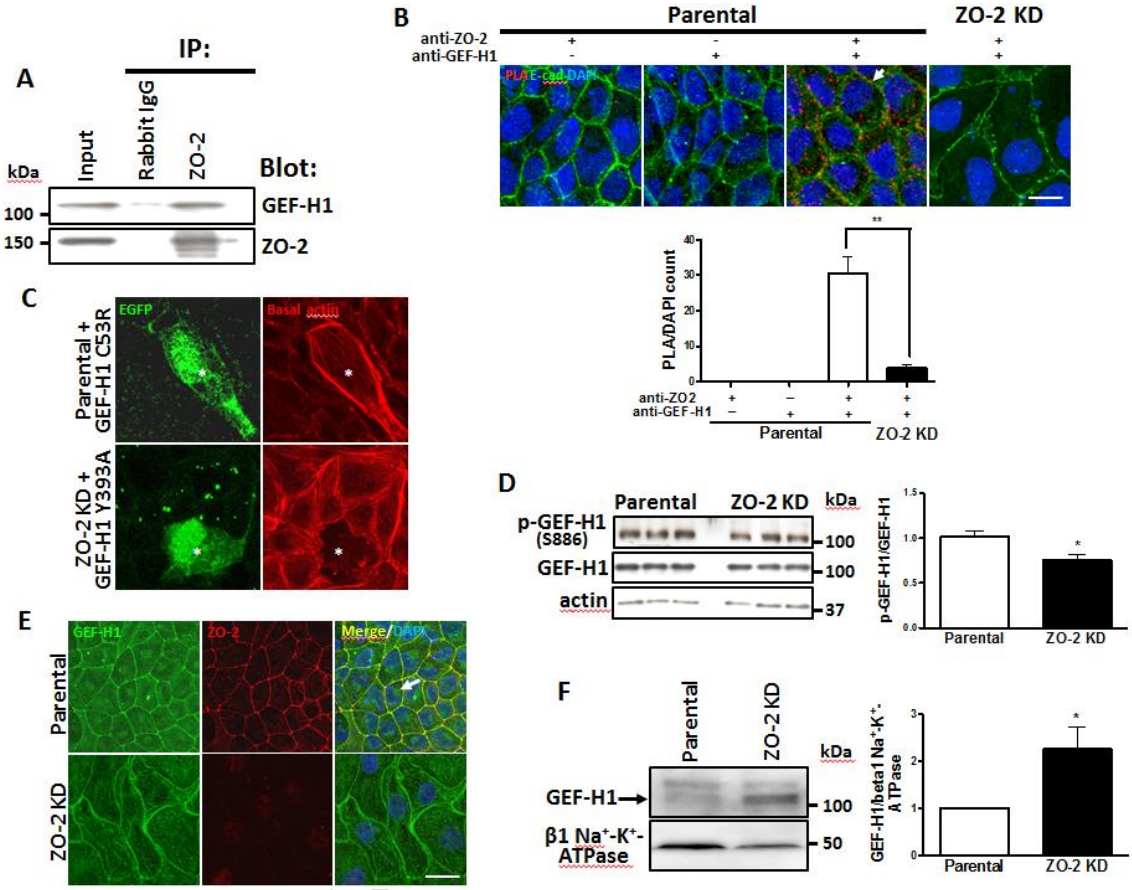

Figure 7

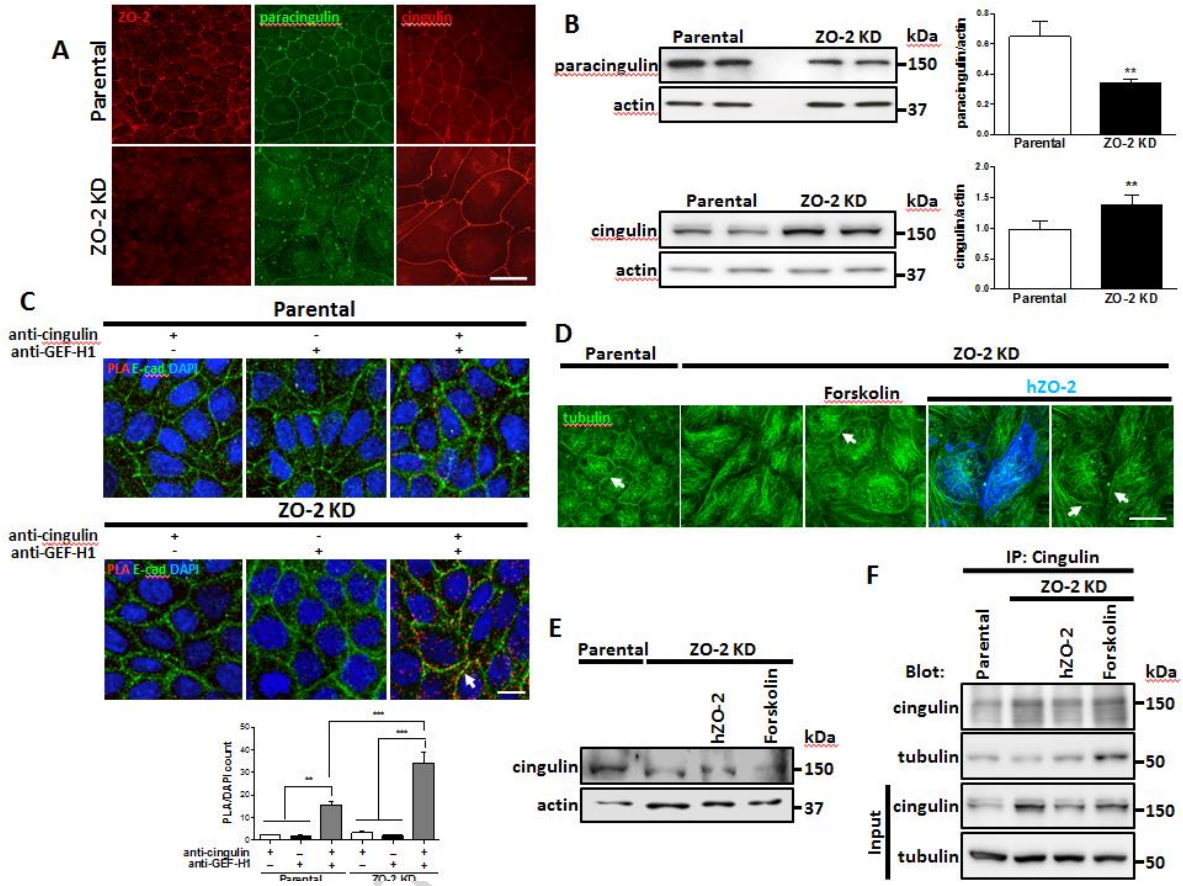

Figure 8

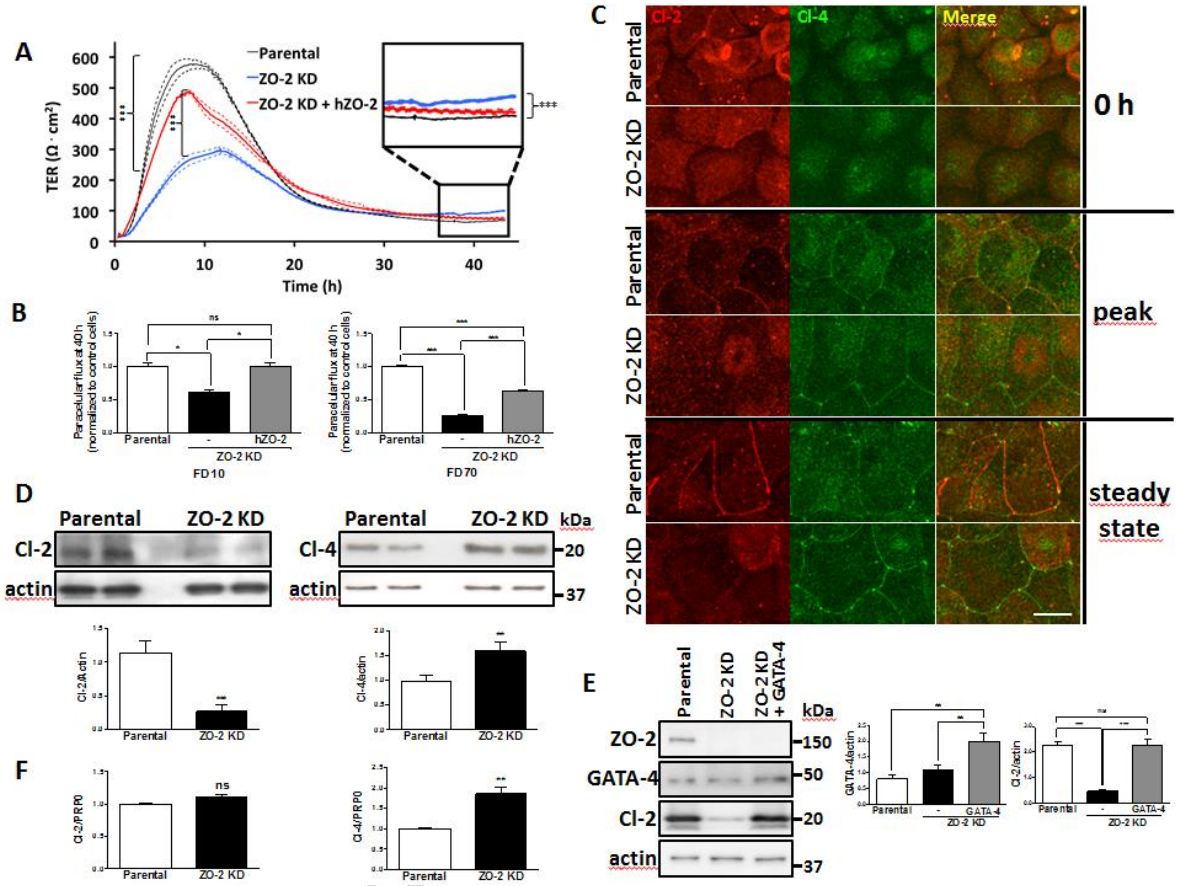

Figure 9

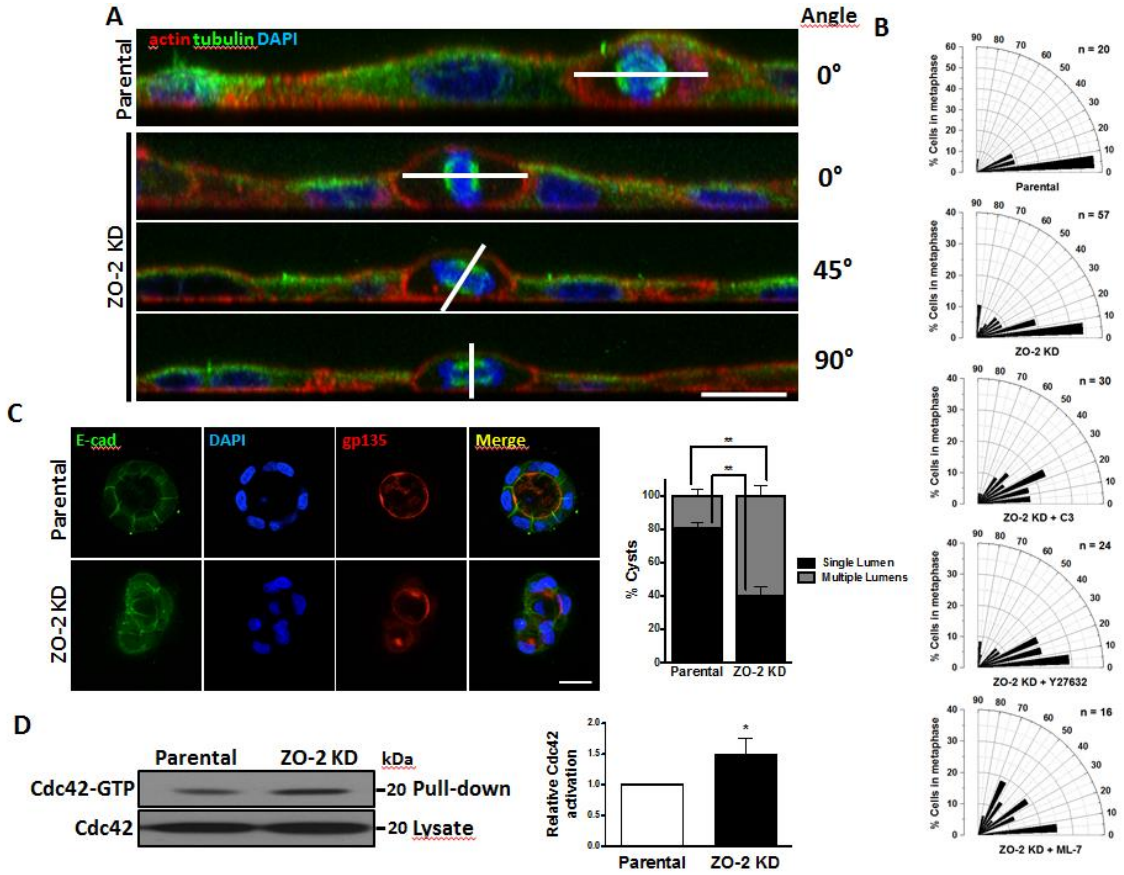

Figure 10

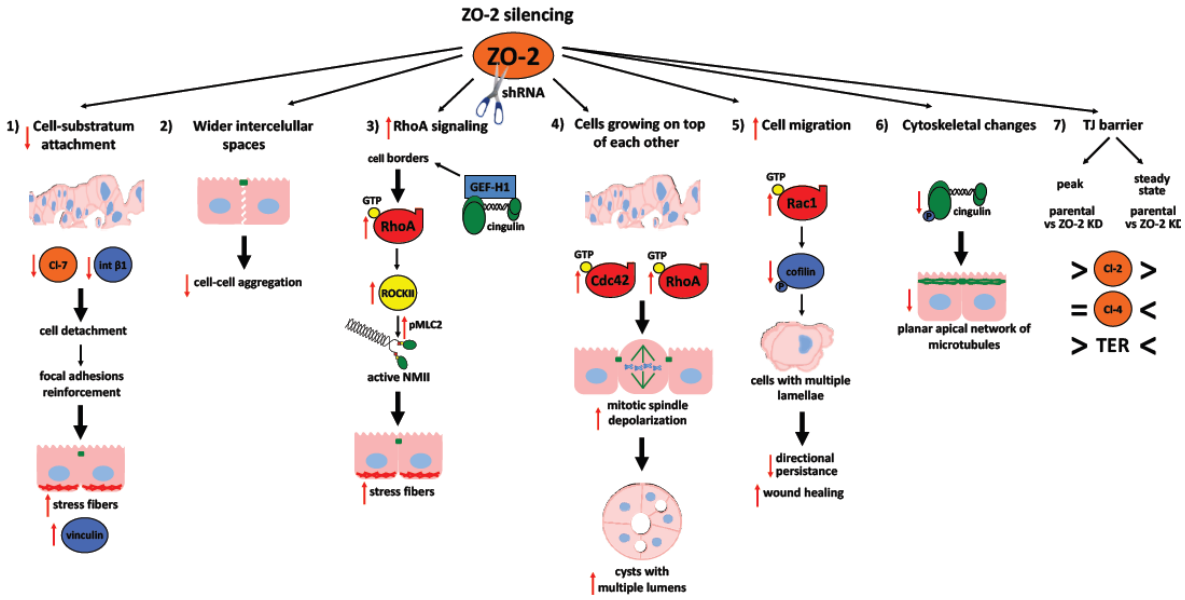

Figure 11

Highlights

1.- Silencing tight junction protein ZO-2 alters epithelial cytoarchitecture.
2.- ZO-2 silencing increases RhoA activity through GEF-H1 recruitment to cell borders.
3.- ZO-2 silencing activates Cdc42 and triggers mitotic spindle disorientation.
4.- ZO-2 silencing increases Rac1 and cofilin activity and lamellipodia formation.
5.- ZO-2 silencing disappears planar apical network of microtubules.